Abiotic hydrogen generation from biotite-rich granite: A case study of the Soultz-sous-Forêts geothermal site, France

Jesica Murray, Alain Clément, Bertrand Fritz, Jean Schmittbuhl, Vincent Bordmann, Jean-Marc Fleury

Applied Geochemistry 119 (2020) 104631

Contents lists available at ScienceDirect

Applied Geochemistry

journal homepage: http://www.elsevier.com/locate/apgeochem

Abiotic hydrogen generation from biotite-rich granite: A case study of the Soultz-sous-Forêts geothermal site, France

Jesica Murray [a,b,*], Alain Clément [a], Bertrand Fritz [a], Jean Schmittbuhl [c], Vincent Bordmann [d], Jean Marc Fleury [d]

[a] LHYGES, Université de Strasbourg, EOST, CNRS, 1 rue Blessig, 67084, Strasbourg, France
[b] CONICET, Instituto de Bio y Geo Ciencias del NOA, Universidad Nacional de Salta, Av. 9 de Julio 14, Rosario de Lerma, Salta, Argentina
[c] IPGS, Université de Strasbourg, EOST, CNRS, 5 rue René Descartes, 67084, Strasbourg, France
[d] TOTAL, 2 place Jean Millier, La Défense 6, 92400, Courbevoie, France

ARTICLE INFO

Handling editor. Dr M Liotta

Keywords:
Native hydrogen
Granitic basement
Biotite oxidation
Geochemical modelling
KIRMAT
Enhanced geothermal system

ABSTRACT

Investigations on geochemical processes involved in H_2 generation in natural reservoirs are important for the present energy transition from fossil fuels. Most studies related to native H_2 focus on the serpentinisation of ultramafic rocks, in which the source of H_2 is linked to oxidation of Fe^{2+}-bearing minerals and a reduction of H_2O. In this study, we investigate abiotic H_2 generation from a biotite-rich granite using an approach based on a study case of the Soultz-sous-Forêts geothermal site in France. Using a geochemical and reactive transport model and an existing database, we simulated the hydrothermal alteration of the granite at 130–200 °C with a redox potential from −100 mV to −300 mV. The simulations show that generation of native H_2 is possible in an open system by hydrothermal alteration of biotite as a source of Fe^{2+}, which oxidises to Fe^{3+} leading to precipitation of Fe^{3+} minerals and reduction of H^+. The amount of H_2 produced depends on the type of $Fe^{2+/3+}$ minerals which precipitate. The optimal conditions for H_2 generation are related to magnetite precipitation as in the serpentinisation process. We assessed that the upper bound for H_2 production for this site is 102 kt per km^3 of granite. This is in case of complete oxidation of all the ferrous iron contained in the biotite of the geothermal reservoir. In practice, only part of this potential may be attained owing to the limited current exploitation methods which are unlikely to result in a complete disequilibrium of the whole biotite. Future research needs to focus on how to reach most of the H_2 potential. Simulations with increasing CO_2 pressures suggest that CO_2 injection can stimulate the H_2 production. This study has implications for possible coupling of heat extraction and future exploitation with H_2 production.

1. Introduction

In the new world scenario of global warming and energy transition from fossil fuels, new CO_2-free energy sources are necessary. Hydrogen-gas (H_2) can play an important role as either an energy vector or a zero-carbon source of energy. Research on native H_2 generation has been conducted in different contexts such as the origin of life in submarine environments, the serpentinisation process, and methanogenesis (Charlou et al., 2002; Kelley et al., 2005; McCollom and Seewald, 2013; McDermott et al., 2015; Etiope et al., 2017; Vacquand et al., 2018). The generation process of H_2 by serpentinisation in mid-oceanic ridges or in ophiolitic systems has been studied most often. Several geochemical modelling and batch laboratory experiments using ultramafic rocks have been conducted to better understand and explain the H_2 generation that occurs during the serpentinisation process (McCollom and Bach, 2009; Klein et al., 2009, 2013; McCollom et al., 2016; Mügler at al., 2016; Miller et al., 2017; Bachaud et al., 2017). Such studies indicate that serpentinisation promotes the formation of H_2 under strongly reducing conditions in which water is reduced to form H_2 as Fe^{2+} is oxidised to Fe^{3+} and is then precipitated in secondary minerals. The generation of H_2 during the serpentinisation process can be represented by reaction 1 (R1) as follows (Klein et al., 2013):

$$(Mg,Fe)_2SiO_4 + vH_2O = w(Mg,Fe)(OH)_2 + x(Mg,Fe)_{3-Fe(III)}(SiFe)_{2-Fe(III)}O_5(OH)_4 + y\ Fe_3O_4 + zH_2 \quad (R1)$$

(olivine + water = brucite + serpentine + magnetite + H_2)

* Corresponding author. 10 rue de Verdun, 67000, Strasbourg, France.
E-mail addresses: murray.jesica@gmail.com, murray.jesica@conicet.gov.ar (J. Murray).

https://doi.org/10.1016/j.apgeochem.2020.104631
Received 28 May 2019; Received in revised form 30 April 2020; Accepted 4 May 2020
Available online 3 June 2020

Other crustal contexts in which abiotic H_2 is generated have been explored less often. An example of this is the Precambrian continental crust. Sherwood Lollar et al. (2014) reported that abiotic processes such as radiolysis and hydration of the Precambrian continental lithosphere (also rich in mafic minerals) have caused global H_2 production rates comparable to those from serpentinisation. Other examples include Precambrian crust fracture systems and thinned-crust basins such as failed-arm rifts, where H_2 is associated with the serpentinisation of deep crust and an alkaline igneous complex (Apps and van de Kamp, 1993; Smith et al., 2005, 2014; Larin et al., 2015; Zgonnik et al., 2015; Guélard et al., 2017).

In the present study, we explore specific reactions that could lead to native abiotic H_2 generation by hydrothermal alteration of a biotite-rich granite using an approach based on a case study of the deep granitic basement of the Soultz-sous-Forêts geothermal site in the Upper Rhine Graben, France (Fig. 1a). The Soultz-sous-Forêts site hosts an enhanced geothermal system in which three deep wells 5000 m in depth have been drilled into the granite basement to create a heat exchanger to produce electricity (Fig. 1b; Bresee, 1992; Gérard et al., 2006; Genter et al., 2010; Huenges and Ledru, 2011; Olasolo et al., 2016; Lu, 2018). Several studies indicate the presence of H_2 at 0.25–46.3 vol% in the gas phase of hydrothermal fluids (e.g. Sanjuan et al., 2010). However, its origin is poorly understood, with some interpretations relating its origin to reactions between the metal tubing material and the brine (Naumann et al., 2000; Pauwels et al., 1993). Our study focuses on biotite-rich granites in which specific primary and secondary minerals have the potential to be oxidised to reduce available protons and produce H_2. This process is similar to that occurring in serpentinisation, in which the oxidation of Fe^{2+} minerals leads to H_2 generation. The objective of this study is to explore the possibilities of abiotic H_2 generation by hydrothermal alteration of the biotite-rich granite at the Soultz-sous-Forêts site with focus on the alteration of biotite. We use an approach based on geochemical and reactive transport modelling to simulate the reactions between the granite and the in situ saturation of the deep hot brine. The abundant data available for this site enabled us to build and calibrate our conceptual model and to investigate the effects of temperature, redox conditions, and partial pressure of CO_2 (PCO_2) variations on H_2 generation. Simulations increasing PCO_2 values were performed to simulate artificial injection of CO_2.

In this study, we verify whether H_2 generation is enhanced by anthropogenic forced circulations of deep geothermal fluids designed for heat extraction. Accordingly, we focus on the potential production of H_2 considering only fluid–mineral interactions and assuming no interaction between the CO_2 and H_2 phases. This configuration assumes that the H_2 phase is trapped in a volume that is spatially different from that of the CO_2 phase. However, both phases, whether in gas, liquid, or supercritical states, are expected to be in contact with the same mobile aqueous phase. A future study will address the possible mixing of the phases if the storage volume is common for both phases. In this case, the combination of CO_2 with H_2 could lead to CH_4 formation following Fischer–Tropsch-type (FTT) reactions (Etiope and Sherwood Lollar, 2013).

2. Geological setting

The Soultz-sous-Forêts site was proposed in the late 1980s as a deep geothermal energy pilot site (Villemin and Bergerat, 1987; Bresee, 1992; Le Carlier et al., 1994; Gérard et al., 2006; Genter et al., 2010; Huenges and Ledru, 2011, Olasolo et al., 2016; Lu, 2018). This site exhibits a high heat flux related to a large temperature gradient up to 110 °C/km in the first kilometre of depth (Pribnow and Schellschmidt, 2000). The temperature at depths of 2000–5000 m in the geothermal reservoir, which consists of fractured granite (Fig. 1b), is 130–200 °C according to the temperature logs of deep wells GPK2, GPK3, and GPK4 (Schindler et al., 2010; Vallier et al., 2019).

Below a Triassic–Quaternary sedimentary sequence of 1400 m in thickness, the basement is composed of three different types of Carboniferous granite, of which porphyritic granite is the most abundant

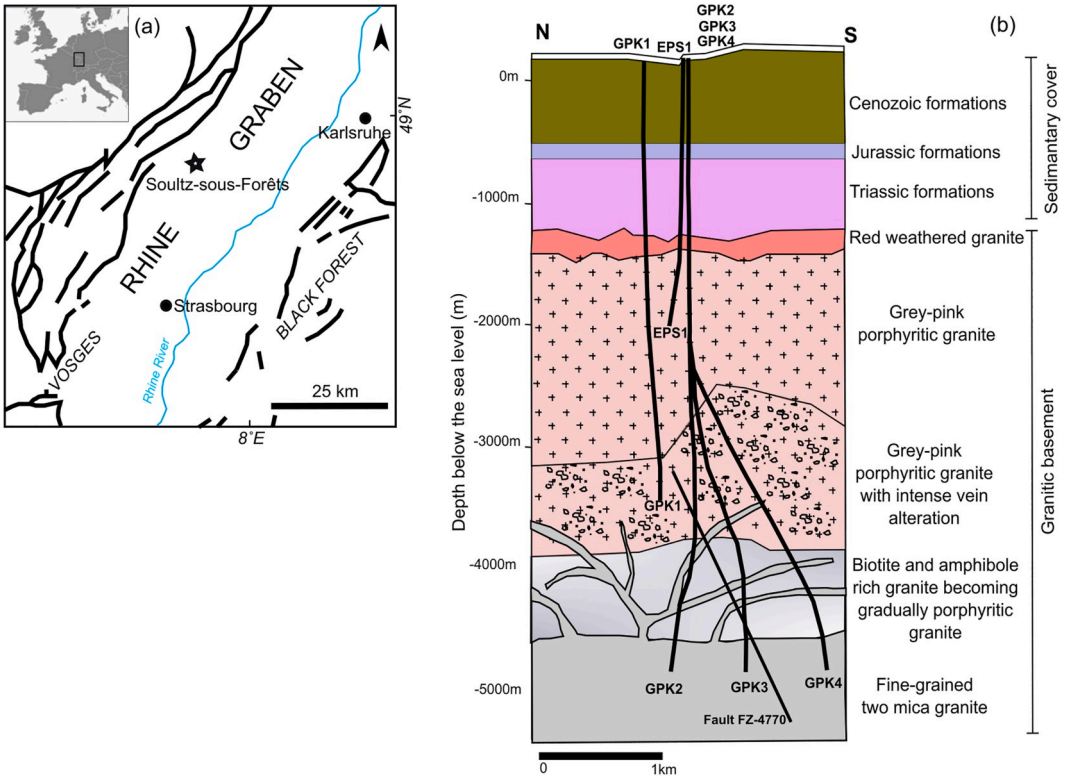

Fig. 1. (a)-Location of the Soultz-sous-Forêts site in the Upper Rhine graben, France (after Sanjuan et al., 2010). (b)- Lithology profile with depth including the trajectories of the boreholes (EPS1, GPK1 to GPK4) and the major fault of the reservoir (FZ-4770) (after Vallier et al., 2019 and Dezayes et al., 2005).

(Fig. 1 b). All granites have abundant biotite and show different grades of fractured and hydrothermal alteration (Hooijkaas et al., 2006; Dezayes et al., 2005). Two main types of hydrothermal alteration have been identified: propylitic and vein alterations (Traineau et al., 1991; Genter and Traineau, 1992; Ledésert et al., 2010 ; Hooijkaas et al., 2006). The propylitic alteration is related to the last stage of granite crystallisation. It occurs in the granitic matrix and is characterised by replacement of biotite and hornblende with chlorite (chamosite) and transformation of plagioclase into illite, sericite, and calcite. Epidote and hydrogarnet are also present. The vein alteration process is related to water–rock interaction that occurred in the natural fractured system. It strongly modifies the petrographic and petrophysical characteristics of the granite, in which illite, haematite, goethite, quartz, carbonates, and sulphides are typical secondary minerals (Traineau et al., 1991).

The granite hosts a strongly saline Na–Cl brine with total dissolved solids (TDS) values at 99–107 g/l, pH values close to 5, and a maximum temperature of 200 °C measured in situ at 5000 m in depth (Sanjuan et al., 2010, 2016). The brine is believed to have multiple origins including a mixture of dilute meteoric water and primary brine formed by advanced evaporation of seawater until the halite precipitation stage, with contributions from halite dissolution following successive marine transgression–regression cycles from the Triassic to the Oligocene (Sanjuan et al., 2010, 2016). This geothermal fluid likely originated from Triassic sedimentary formations located at great depth (≥4 km) with temperatures close to 225 ± 25 °C in the centre of the Rhine Graben. The He isotopic signatures of the gases associated with these fluids indicate that the thermal anomalies are mainly crustal and not mantle-derived (Sanjuan et al., 2016). According to the U–Th isotope system, the minimum transit time of these deep geothermal brines is about 1000 years (Sanjuan et al., 2016).

In general, the brine has quantities of gas in which the gas/liquid volume ratio at 20 °C and 25 °C is ~20% or higher (Sanjuan et al., 2010, 2016). Among the gases, CO_2 with an apparent mixed sedimentary–mantle origin is dominant, at 14.2–89.7 vol % (Sanjuan et al., 2016), followed by N_2 at 7.2–48.6 vol %, H_2 at 0.83–46.3 vol %, CH_4 at 1.2–6.8 vol %, and He at 0.45–2.2 vol %. No trace of H_2S was found (Sanjuan et al., 2010, 2016).

3. Modelling approach

3.1. Conceptual model and modelling strategy

To test the generation of H_2 by hydrothermal alteration of the granite basement at Soultz-sous-Forêts, we simulated the circulation of the hydrothermal Na–Cl brine through a 1 m^3 cube of fresh porphyritic granite considered to be a representative reactive cell (Fig. 2). We selected porphyritic granite as the reactive rock because this type is the most abundant granite at the site. The 'fresh' designation assumes the granite contains no prior propylitic or vein hydrothermal alterations.

Fig. 3 illustrates the simulations performed in this work. We began with a 'reference simulation' considering the composition of a brine at 165 °C and an initial Eh of −245 mV as calculated by Fritz et al. (2010) for the brine circulating at 3500 m depth in the porphyritic granite domain (Table 1). In subsequent steps, were tested the effects of temperature, redox conditions, and PCO_2 on H_2 generation (Fig. 3). The effect of temperature was evaluated by exploring the minimum and maximum temperatures of the site, respectively at 130 and 200 °C, using an initial Eh equal to that of the reference simulation, at −245 mV. In the simulations, the initial Eh value is given as an input parameter. However, this value can vary during simulation depending on the evolution of the solution composition. The effect of the redox potential was tested using the maximum and minimum values, respectively at −100 mV and −300 mV as initial Eh while maintaining constant temperature at 165 °C. The upper limit of −100 mV for the Eh corresponds to the value estimated by Sanjuan et al. (2010), whereas −300 mV is the lowest value calculated by Fritz et al. (2010). Finally, simulations combining the entire range of temperatures and Eh values were conducted with temperature and Eh increments of 10 °C of −50 mV, respectively.

All simulations were conducted considering an open system with respect to the solution and the gas phases. The PCO_2 value in the geothermal system was calculated from the pH and alkalinity of the brine, at 4.8 and 15 meq/kg, respectively (Fritz et al., 2010), according to the thermodynamic equilibrium condition represented in Eq. (1), where $[H^+]$ is the activity of protons, $[CO_3^{2-}]$ is the activity of dissolved carbonate, and K CO_2 is the equilibrium constant for reaction 2 (R2):

$$[PCO_2] = [H^+]^2\,[CO_3^{2-}]/[KCO_2]\,[H_2O] \quad [1]$$

$$CO_2(g) + H_2O \rightarrow 2H^+ + CO_3^{2-} \text{ (R2)}.$$

The calculated PCO_2 was 0.1 MPa. To evaluate the effect of increased CO_2 in the system as well as its effect on H_2 production, simulations were conducted with increasing values of PCO_2. As such, the initial value of alkalinity was increased successively from 15 meq/kg to 30 meq/kg, 60 meq/kg, and 90 meq/kg (Fig. 3).

In this framework, the partial pressure of H_2 (PH_2) is assumed to be constant during the simulations. Under thermodynamic equilibrium, P_{H2} is determined at the beginning of the simulation from the initial Eh and pH, represented in Eq. [2] by the activities of protons $[H^+]$ and electrons $[e^-]$. Reaction 3 (R3) describes H_2 generation in equilibrium with a given equilibrium constant (KH_2):

$$[PH_2] = [H^+]^2\,[e^-]^2/K\,H_2 \quad [2]$$

$$H_2 = 2H^+ + 2e^- \text{ (R3)}$$

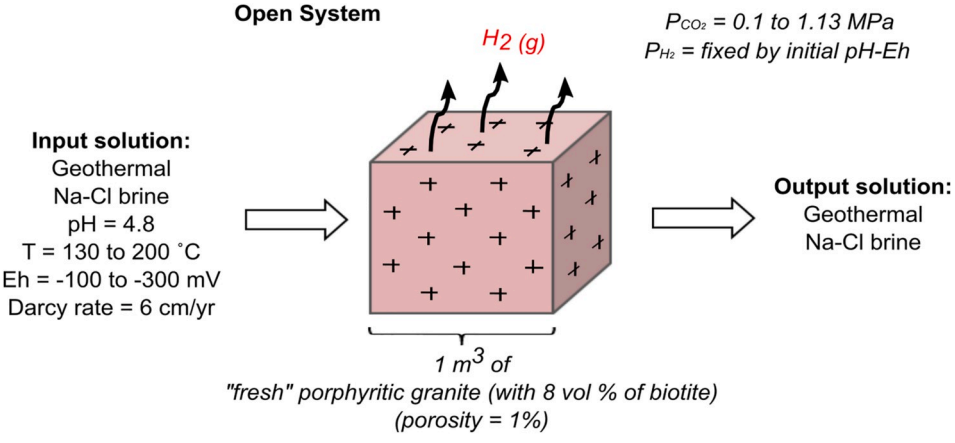

Fig. 2. Conceptual model for geochemical and reactive transport simulations of native H_2 generation in the geothermal reservoir of Soultz-sous-Forêts.

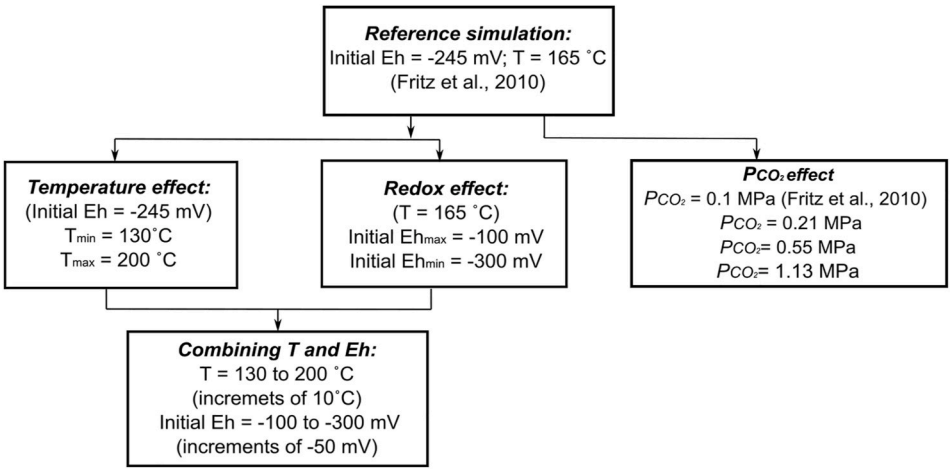

Fig. 3. Diagram illustrating the simulations performed with KIRMAT for H_2 production in the geothermal reservoir of Soultz-sous-Forêts.

Table 1
Initial composition of the hydrothermal brine considered in this model after Fritz et al. (2010). The concentration of Fe and Al were decreased one and two orders of magnitude respectively in order to prevent initial oversaturation of some secondary minerals.

Parameter	Molality (mMol/Kg H_2O)
Na	1190
K	65.5
Ca	166
Mg	4.17
Cl	1580
Fe	0.0116
Al	7.44 E−05
Alkalinity	15 (meq/Kg)
Si	1.8
Temperature	165 (°C)
pH	4.8
Eh	−245 (mV)

The concentration of O_2 was considered to be very low because we simulated conditions at depths greater than 3000 m below the surface. The concentrations of N_2, CH_4, and He were neglected to simplify the simulations.

3.2. Kinetics of Reaction and Mass Transfer code

Simulations were conducted using the Kinetics of Reaction and Mass Transfer (KIRMAT) numerical code, which couples chemical reaction and mass transfer (Gérard et al., 1998). This code simulates the geochemical reactions that occur during one-dimensional (1D) circulation of a fluid through a determined reactive cell to evaluate changes in the mineral composition, porosity, permeability, temperature, Darcy velocity, fluid–rock interaction, thermodynamic equilibrium, precipitation and dissolution of minerals. The code also accounts for the feedback effects of the chemical and mineralogical evolutions on the variation of porosity. The KIRMAT code is monophasic, which means that it resolves the mass balance equations for transport associated with geochemical reactions in the liquid phase but does not simulate the transport of the gas produced by the reactions. In open systems, any gas produced is exported outside from the reactive cell (Fig. 2).

3.2.1. Kinetic data

To calculate the dissolution rates of the primary minerals at different pH values KIRMAT uses the following reaction:

$$r_d = k_d S^{eff}_m a^n_{H+} [\,1 - ((Q_m/K_m)^{na})^{nb}] \quad [3]$$

where r_d is the dissolution rate of a mineral m (mol year^{-1} kg$^{-1}_w$); k_d is the dissolution rate constant (mol m^{-2} year^{-1}; Table 2); S^{eff}_m is the reactive surface area of the mineral (m^2 kg$^{-1}_w$); a_{H+} is the activity of protons; n is an experimental power, where n_a and n_b are experimental exponents depending on the pH of the solution; Q_m is the ion activity product of the mineral for a given composition of the aqueous solution; and K_m is the equilibrium constant for the hydrolysis reaction of the mineral at a given temperature and pressure.

For the kinetic precipitation of minerals, KIRMAT code considers the following expression:

$$r_p = k_p S^{eff}_m [(Q_m/K_m)^p - 1]^q \quad [4]$$

where k_p is the kinetic rate constant of precipitation (mol m^{-1} year^{-1}), and p and q are experimental values describing the dependence of the reaction on the saturation state (Table 3). The kinetic precipitation approach was used for quartz at temperatures lower than 150 °C in which the initial oversaturation of the mineral was detected by calculating the chemical speciation.

3.2.2. Thermodynamic data

In geochemical modelling, the precipitation of minerals is generally considered to be in thermodynamic equilibrium with the aqueous solution. This premise is made owing to the lack of data for kinetic rate laws of precipitation for many minerals and to the assumption of long-term processes at the geological time scale that would enable the system to return to equilibrium. The thermodynamic data for the minerals selected in this study were taken from the Thermoddem database updated by the French Geological Survey (BRGM Blanc, 2017).

3.3. Input parameters

3.3.1. Primary minerals in the granitic reactive cell

The sets of primary minerals and volume fractions selected for the model are based on the composition of the standard porphyritic granite occurring at the site (Hooijkaas et al., 2006). We consider that the fresh porphyritic granite is composed of plagioclase (albite 35 vol %; anorthite 4 vol %), quartz (27 vol %), K-feldspar (24 vol %), biotite (8 vol %) and amphibole (2 vol %) (Table 4). Biotite is the most important source of Fe^{2+} that accounts for H_2 generation in the basement of the Soultz-sous-Forêts granitic reservoir. Our model uses pure ferrous annite ($KFe^{II}_3(AlSi_3)O_{10}(OH)_2$) as an end-member of the solid solution (Table 4). This approximation was used to calculate the maximum possible amount of Fe^{2+} that could be hosted in biotite and therefore the maximum potential amount of H_2 production.

Table 2
Kinetic constants for dissolution reactions of primary minerals. Data assessed by the authors from Palandri and Kharaka (2004) data base.

	Ka	kn	kb	pH_a	pH_b	n_a	n_b	Ea	En	Eb
	mol m^{-2} $year^{-1}$							kJ/mol		
	T = 130 °C									
Quartz	4.84E+00	1.86E-02	1.43E-04	4.83	5.83	0.5	−0.5	99.2	90.1	108.4
Microcline	6.29E-01	6.67E-04	3.92E-10	5.95	7.60	0.5	−0.82	51.7	38	94.1
Anorthite	5.69E+04	1.55E-01	1.37E-05	3.95	7.11	1.41	−0.57	16.6	17.8	71
Albite	2.02E+00	1.33E-02	1.37E-05	4.74	5.24	0.46	−0.57	65	69.8	71
Annite	4.64E-02	8.96E-05	8.96E-07	5.12	9.09	0.53	−0.22	22	22	22
Tremolite	9.14E-01	1.61E+01	–	–	–	–	–	18.9	9.44	–
	T = 165 °C									
Quartz	5.15E+01	1.59E-01	1.90E-03	5.02	6.02	0.5	−0.5			
Microcline	2.16E+00	1.65E-03	3.69E-09	6.23	6.89	0.5	−0.82			
Anorthite	8.46E+04	2.37E-01	7.46E-05	3.94	6.14	1.41	−0.57			
Albite	9.49E+00	7.00E-02	7.46E-05	4.64	5.21	0.46	−0.57			
Annite	7.84E-02	1.51E-04	1.51E-06	5.12	9.09	0.53	−0.22			
Tremolite	1.43E+00	1.52E+02	–	–	–	–	–			
	T = 200 °C									
Quartz	3.86E+02	9.93E-01	1.71E-02	5.18	6.18	0.5	−0.5			
Microcline	6.16E+00	3.57E-03	2.49E-08	6.47	6.29	0.5	−0.82			
Anorthite	1.18E+05	3.40E-01	3.16E-04	3.93	5.32	1.41	−0.57			
Albite	3.55E+01	2.89E-01	3.16E-04	4.54	5.20	0.46	−0.57			
Annite	1.23E-01	2.37E-04	2.37E-06	5.12	9.09	0.53	−0.22			
Tremolite	2.11E+00	1.04E+03	–	–	–	–	–			

a = acid mechanism.
n = neutral mechanism.
b = basic mechanism.
E = Arrhenius activation energy.
Note: Due to the lack of valid data of pH limits for tremolite, only kd for acid conditions was used during the simulations.

Table 3
Kinetic constants for precipitation of secondary minerals.

	Kp	p	q
Mineral	mol m^{-2} $year^{-1}$		
Quartz	1.16E-01 (130 °C)	1	1
Quartz	1.67E-01 (140 °C)	1	1

Kinetic constants were calculated following the micro-reversibility law using data from Ganor et al. (2005) and Rimstidt and Barnes (1980).

Table 4
Primary minerals of the granite considered in this study. The ideal stoichiometry is taken from the Thermoddem (BRGM) data base (June-2017). The volume fraction values were taken from the descriptions of the porphyritic granite. Plagioclase is described as albite and anorthite end-members.

Primary mineral	Stoichiometry	Volume fraction (%)
Quartz	SiO_2	27
Feldespar- K	$K(AlSi_3)O_8$	24
Anorthite	$Ca(Al_2Si_2)O_8$	4
Albite	$Na(AlSi_3)O_8$	35
Biotite (annite)	$KFe^{II}_3(AlSi_3)O_{10}(OH)_2$	8
Amphibole (tremolite)	$Ca_2Mg_5Si_8O_{22}(OH)_2$	2

3.3.2. Secondary minerals by hydrothermal alteration of the granite

Secondary minerals are those precipitated by hydrothermal alteration of the fresh granite during the simulations. We selected a set of secondary minerals that have been previously identified in the two types of hydrothermal alteration of the granite, i.e. propylitic and vein alterations (Table 5). The number of minerals considered in the simulations should not force the reaction pathways. Accordingly, we introduced numerous phases for the Fe secondary minerals: Fe^{2+} phases including nontronite, chamosite, and epidote; Fe^{3+} phases including haematite and goethite; and Fe^{2+}/Fe^{3+} phases including magnetite (Table 5). Thus if the dissolution of biotite is achieved and Fe^{2+} is released to the solution, the code will choose between the precipitation of Fe^{2+} and Fe^{3+} secondary minerals according to the Fe speciation (Eh–pH conditions) and the saturation indices of the minerals.

Table 5
Secondary minerals selected for this study, based on the description of vein and propylitic alterations at Soulz-sous-Forêts. The ideal stoichiometry was acquired from Thermoddem (BRGM) data base (June-2017).

Secondary mineral	Stoichiometry	Alteration type
Quartz	SiO_2	Vein/propylitic
Illite-Al	$K_{0.85}Al_{2.85}Si_{3.15}O_{10}(OH)_2$	vein
Montmorrillonite (MgCa)	$Ca_{0.17}Mg_{0.34}Al_{1.66}Si_4O_{10}(OH)_2$	vein
Montmorrillonite (MgNa)	$Na_{0.34}Mg_{0.34}Al_{1.66}Si_4O_{10}(OH)_2$	vein
Nontronite (K)	$K_{0.34}Fe_{1.67}Al_{0.67}Si_{3.66}O_{10}(OH)_2$	vein
Magnetite-III	$Fe^{III}_2\,Fe^{II}O_4$	vein
Haematite-III	$Fe^{III}_2O_3$	vein
Goethite-III	$Fe^{III}O(OH)$	vein
Epidote	$Ca_2Fe^{III}Al_2Si_3O_{12}(OH)$	propylitic
Chamosite (Chlorite group)	$Fe^{II}_5Al(AlSi_3)O_{10}(OH)_8$	propylitic
Kaolinite	$Al_2Si_2O_5(OH)_4$	vein
Calcite	$CaCO_3$	propylitic
Dolomite	$CaMg(CO_3)_2$	vein
Beidellite-K	$K_{0.34}Al_{2.34}Si_{3.66}O_{10}(OH)_2$	vein

To reduce the complexity of the system related to redox reactions caused by S species, the simulations were made without considering sulphide and sulphates in the sets of secondary phases.

3.3.3. Composition of the geothermal brine

Very little research analyzed the deep geothermal fluids at Soultz-sous-Forêts with no contamination by drilling fluids or injected water (Sanjuan et al., 2010, 2016). In the case of the fluids extracted with a deep auto-sampler, it could have experienced changes between the in situ reservoir and ex situ lab conditions caused by i) equilibration with atmospheric conditions and dissolution of atmospheric O_2 with strong evolution of redox conditions after extraction and sampling; ii) strong temperature evolution between ~165 °C at depth and 20 °C in the lab; iii) CO_2 degassing and consequent evolutions of pH and alkalinity in the presence of carbonate precipitation. Therefore, the composition of the fluid used in this study corresponds to the values calculated by Fritz et al. (2010) at thermodynamic equilibrium with the mineral phases of the partly cemented hydrothermalised granite facies (Table 1). The

calculations were based on the composition of the hydrothermal fluid at 165 °C and pH = 4.8 measured at 3500 m in depth during the 1997 circulation test with no contact with the atmosphere.

To calculate the activity coefficients of the ions, the extended Debye–Hückel law was used. It could be argued that simulations with heavy brine should include Pitzer equations; however, this approach can be applied only in geochemical models for major ions at low or intermediate temperatures. In our case, calculations for aqueous trace element activities (Al^{3+}, Fe^{2+}, Fe^{3+}) were needed because they are crucial for simulating iron and clay mineral–solution interaction. For this reason, we considered that the extended Debye–Hückel law was a better method for calculating the ion activity. In our simulations, the ionic strength values remained almost constant at ≈1.5, which limited the risk of cumulative error.

3.3.4. Reactor size, porous media, and reactive transport parameters

The volume of rock in the simulation was 1 m^3, which is considered to be a relevant scale for describing the fault network and the major fault thickness in which the fluid circulation is expected to be active. In the simulation, we considered a proxy of the natural fractured granite as a reactive cell in which the minerals and the porosity were homogeneously distributed throughout the volume (Fig. 2). The average porosity was set to 1% because the porosity of the granite at Soultz-sous-Forêts varies at a wide range of 0.1–10%, where the lowest values correspond to the less-altered zones of the granite, and the highest values correspond to high pervasive and vein alteration zones (Kohl et al., 1995; Surma and Géraud, 2003; Rosener and Géraud, 2007; Magnenet et al., 2014). The Darcy velocity selected for this simulation was 6 cm/yr which is a characteristic value of the Darcy velocity distribution in the hydrothermal system (Vallier et al., 2019). The maximum time of the simulation was 250 years. Rather than reproducing long-term geological processes of thousands to millions of years, the duration of the simulation was designed to reproduce shorter time scales related to the geothermal exploitation of the wells, at tens to hundreds of years.

3.3.5. Reactive surface area of primary minerals

In this study, the reactive surface areas of the primary minerals *m* ($S^{EFF}{}_m$ in m^2/kg_{H2O}) were calculated using Eq. (5) with the specific surface area of the granite (Ss_g in m^2/m^3 of rock) measured by Rosener and Géraud (2007), the volume fraction (Vf_m) of each primary mineral, and the granite porosity (ω):

$$S^{EFF}{}_m = Vf_m * (Ss_g)/(1000 * \omega) \quad [5]$$

The $S^{EFF}{}_m$ values calculated for the primary minerals are shown in Table 6 and were considered as constant during the simulation. The 1000 conversion factor in Eq. (5) was used to convert the aqueous solution from cubic metres to cubic decimetres.

Table 6
Reactive surface of primary minerals calculated with a specific surface of the granite of 2.90E+05 $m^2\ m^{-3}$ and a porosity of 1%.

Primary mineral	$S^{EFF}{}_m$ (m^2/Kg_{H2O})
Quartz	7830
K-Feldspar	6960
Albite	9860
Anorthite	1160
Annite	2320
Tremolite	580

4. Results

4.1. Production of H_2 at 165 °C and −245 mV

Generation of H_2 was observed in the reference simulation, in which the brine circulated through the granitic reactor at T = 165 °C and an initial Eh value of −245 mV (Fig. 4a). The Fe-bearing mineral phases involved in the generation of H_2 were biotite and magnetite (Fig. 4b and c). Biotite dissolves and releases Fe^{2+} to the solution. In an aqueous solution, the partial or total oxidation of Fe^{2+} to Fe^{3+} provides electrons (e^-) (R4) which in an O_2-free environment will reduce protons (H^+) and produce H_2 (R5 and R6).

$$Fe^{2+} \rightarrow Fe^{3+} + e^- \quad (R4)$$

$$H_2O \leftrightarrow H^+ + OH^- \quad (R5)$$

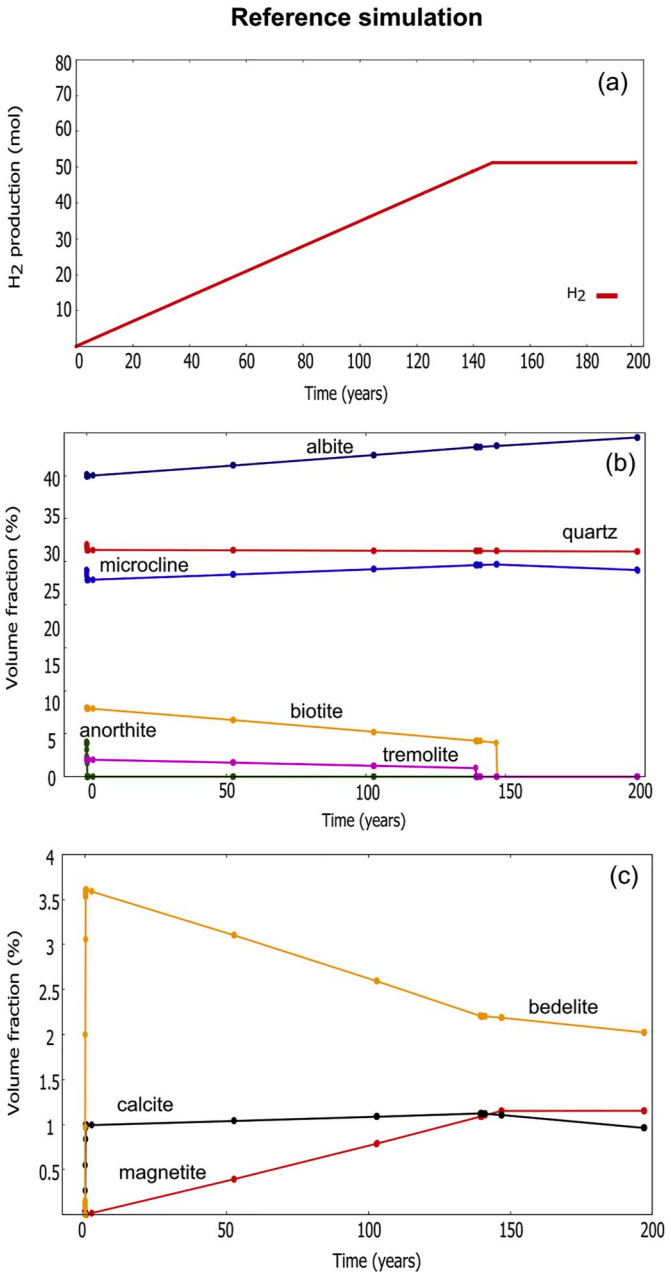

Fig. 4. Results of the reference simulation with a brine at T = 165 °C and Eh = -245 mV. (a)- Production of H_2. (b)- Volume fraction variation for primary minerals. (c)- Volume fraction variation for secondary minerals.

$H^+ + 1e^- \leftrightarrow 0.5H_2$ (R6)

In other terms, H_2 is produced by the reduction of protons provided by the dissociation of water. Because of the increase of Fe^{2+} or Fe^{3+} activities in solution owing to biotite dissolution, secondary Fe-bearing minerals can precipitate. Depending on the degree of oxidation of the aqueous Fe and the type of secondary mineral precipitated, the amount of H_2 produced can vary widely:

(1) Total oxidation of aqueous Fe^{2+}:

1 mol of biotite ($KFe^{2+}_3(AlSi_3)O_{10}(OH)_2$) dissolved →

1 mol of haematite (Fe^{3+}_2 O_3) or goethite ($Fe^{3+}O(OH)$) precipitated + 1.5 mol of H_2 produced (R7)

(2) Partial oxidation of aqueous Fe^{2+}:

1 mol of biotite ($KFe^{2+}_3(AlSi_3)O_{10}(OH)_2$) dissolved →

1 mol of magnetite ($Fe^{3+}_2Fe^{2+}O_4$) precipitated + 1 mol of H_2 produced (R8)

(3) No oxidation of aqueous Fe^{2+}:

1 mol of biotite ($KFe^{2+}_3(AlSi_3)O_{10}(OH)_2$) dissolved →

1 mol of chamosite ($Fe^{2+}{}_5Al(AlSi_3)O_{10}(OH)_8$) precipitated + no H_2 produced (R9)

In our reference simulation, we observed the second case (R8) with the formation of magnetite, in which the amount of dissolved biotite and precipitated magnetite influenced the amount of H_2 produced during the simulation. At 165 °C and −245 mV, the total amount of biotite initially present in the reactor, 51.3 mol, was dissolved after about 147 years. All of the Fe released by the biotite was consumed by the precipitation of 51.3 mol of magnetite and the production of a total amount of 51.3 mol of H_2.

4.1.1. Evolution of primary and secondary minerals

In the reference simulation, all primary minerals were initially undersaturated in the solution and were able to dissolve. However, microcline and albite rapidly reached equilibrium and began to precipitate, whereas quartz, biotite, tremolite, and anorthite continued to dissolve over time (Fig. 4b). The anorthite was completely dissolved and removed from the reactive cell very early in the simulation. The dissolution of biotite, which is involved in the H_2 generation process, progressed with time until about 147 years, at which time it was removed completely (Fig. 4b).

Regarding the secondary minerals, beidellite-K, calcite, and magnetite reached equilibrium successively during the simulated circulation of the brine and began to precipitate (Fig. 4c). The precipitation of calcite at the very beginning of the simulation was favoured by the dissolution of CO_2 and the dissolution of anorthite, which is the main source of Ca^{2+} for calcite. Because the precipitation of calcite was limited by the complete dissolution of anorthite, once this mineral was removed from the cell, calcite began to re-dissolve progressively over time induced by CO_2 dissolution (section 4.3). The precipitation of beidellite-K was favoured at the very beginning of the simulation by the initial dissolution of the silicates. However, the beidellite-K formation was limited later by the precipitation of microcline during the simulation. As described in section 4.1, biotite is the source of Fe^{2+}, which was partially oxidised and precipitated in the magnetite. The precipitation of magnetite progressed until about 147 years and ceased because the biotite was completely dissolved in the reactive cell and the source of Fe disappeared, which limited the production of magnetite and consequently the production of H_2.

4.1.2. Evolution of the physical–chemical composition of the brine

The concentration of ions in the solution remained almost constant during the reference simulation (Fig. 5a and b). The changes were observed at the beginning of the simulation when the fluid entered the granitic cell. Once the system was equilibrated, no changes were observed in the amounts of Cl, Si, Al, Na, Ca, K, Mg, and C circulating through the reactive cell during the simulation. Similarly, no changes were observed in the concentrations of Fe^{2+} and Fe^{3+}; the initial concentration of Fe was very low, and the Fe released to the solution by biotite dissolution was immediately precipitated in the magnetite.

At the very beginning of the simulation, the pH became less acidic, evolving from 4.8 to 5.25 but remaining constant and low during the rest of the simulation. This initial pH change is attributed mainly to the initial equilibration with CO_2 and the hydrolysis of silicates (biotite, tremolite, microcline, anorthite, albite) consuming protons (Table 7). Although the production of H_2 contributes to proton consumption throughout the simulation, the pH of the system is mainly controled by the equilibrium between CO_2 and the dissolution of calcite (Fig. 5c). The Eh value became more negative during the simulation, with an initial value of −245 mV to a final value of −285 mV at the end of the simulation (Fig. 5d).

4.2. H_2 generation at different temperatures (T_{min} = 130 °C; T_{max} = 200 °C)

This section describes the effect of temperature on H_2 generation and on the main mineral phases at 130 °C and 200 °C, which are respectively the minimum and maximum temperatures in the geothermal reservoir. At 130 °C and −245 mV, which is the same initial Eh value as that used in the reference simulation, a considerable reduction was noted in the H_2 production. This result is attributed to the type of secondary Fe mineral precipitating in the reactive cell, which in this case was chamosite ($Fe^{2+}{}_5Al(AlSi_3)O_{10}(OH)_8$) (Fig. 6a and b). Under this condition, the Fe^{2+} released from biotite was not oxidised but remained as Fe^{2+} to precipitate as chamosite (R9). Without a source of e^- for the reduction of protons, no H_2 is produced. Moreover, we observed that at 130 °C, the timing for the dissolution of biotite increased to 246 years.

By increasing the temperature to 200 °C and maintaining the initial Eh value of the reference simulation (−245 mV), the dissolution of biotite was faster and was completed in about 91 years. The precipitation of secondary phases such as epidote ($Ca_2Fe^{3+}Al_2Si_3O_{12}(OH)$) was observed at the beginning of the simulation during the first 20 years (Fig. 6c). In this case, the Fe^{3+} released from biotite was oxidised and precipitated as a pure Fe^{3+} phase. The production of H_2 associated with this secondary phase (i.e. the epidote phase) was 5.9 mol. However, its precipitation did not continue over time, and it was re-dissolved in the cell (Fig. 6c). At that point, the magnetite reached equilibrium and precipitated until the end of the simulation as the main Fe secondary mineral. The Fe^{3+} released by epidote was re-used in the system and was precipitated as magnetite, which reached an amount of 51.3 mol at the end of the simulation. The total production of H_2 was 51.3 mol, which is the same amount as that obtained in the reference simulation (R8).

4.3. H_2 generation at different initial Eh (Eh_{max} = −100; Eh_{min} = −300 mV)

The effect of the redox potential on the H_2 generation was studied by comparing simulations at two different initial Eh values set to −100 mV and −300 mV. The temperature was maintained at 165 °C. The complete dissolution of biotite was achieved in 147 years, which is similar to that observed in the reference simulation with an Eh = −245 mV. This result indicates that the dissolution rate is controlled mainly by temperature. With an initial Eh of −100 mV, goethite ($Fe^{3+}O(OH)$) was the main secondary Fe mineral precipitated, which corresponds to a significant increase in H_2 production, from 51.3 mol to 76.9 mol (Fig. 7a and b). In this case, all of the Fe^{2+} released from the biotite was transformed into Fe^{3+}, which changed the stoichiometry of the reaction to 0.5 H_2 mol produced per mol of Fe^{3+} (R7). At Eh = −300 mV, the secondary mineral

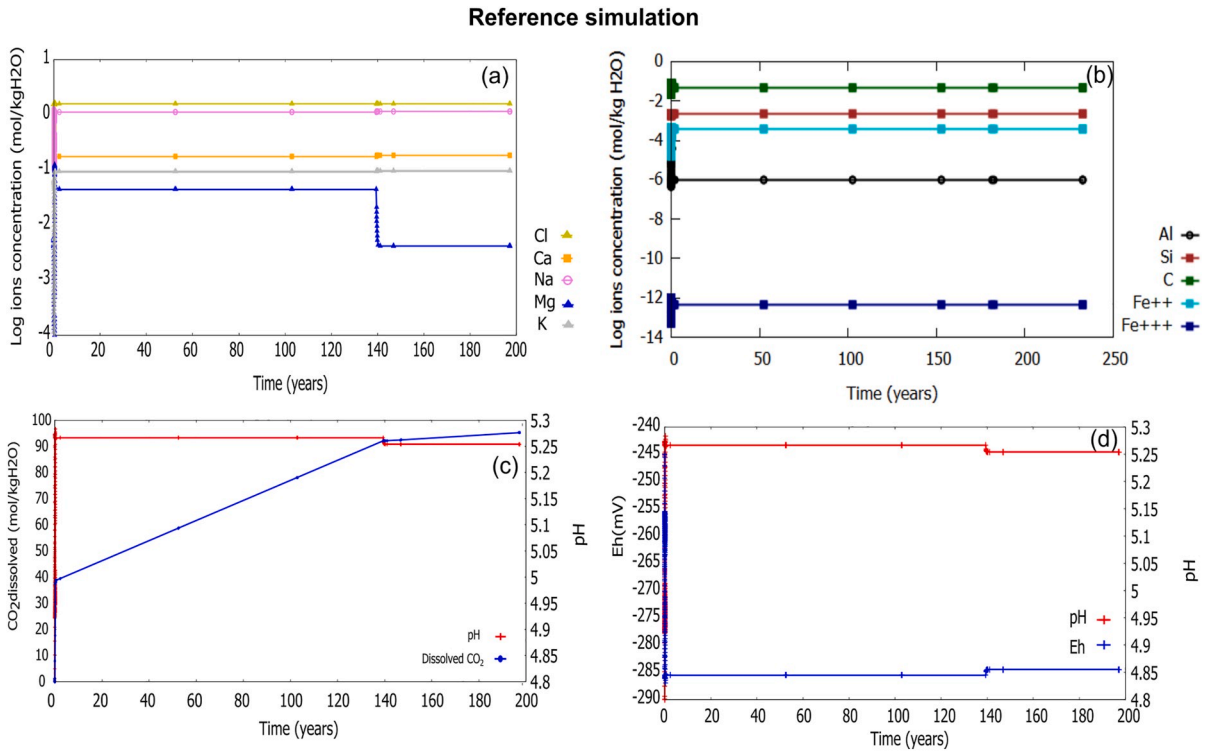

Fig. 5. Evolution of the physical and chemical parameters of the brine during the reference simulation at T = 165 °C and Eh = -245 mV. (a)- Major ions. (b)- Trace elements. (c)- pH and dissolved CO_2. (d)- Eh and pH.

Table 7
Reaction stoichiometry for primary, secondary minerals, and hydrogen.

Mineral	Reactions
Primary minerals	
Quartz	$SiO_2 + 2H_2O \rightleftharpoons H_4SiO_4$
Feldespar- K	$K(AlSi_3)O_8 + 4H^+ + 4H_2O \rightleftharpoons Al^{3+} + K^+ + 3H_4SiO_4$
Anorthite	$Ca(Al_2Si_2)O_8 + 8H^+ \rightleftharpoons 2Al^{3+} + Ca^{2+} + 2H_4SiO_4$
Albite	$Na(AlSi_3)O_8 + 4H^+ + 4H_2O \rightleftharpoons Al^{3+} + Na^+ + 3H_4SiO_4$
Biotite (annite)	$KFe^{II}{}_3(AlSi_3)O_{10}(OH)_2 + 10H^+ \rightleftharpoons Al^{3+} + 3Fe^{2+} + K^+ + 3H_4SiO_4$
Amphibole (tremolite)	$Ca_2Mg_5Si_8O_{22}(OH)_2 + 14H^+ + 8H_2O \rightleftharpoons 2Ca^{2+} + 5\ Mg^{2+} + 8H_4SiO_4$
Secondary minerals	
Illite-Al	$K_{0.85}Al_{2.85}Si_{3.15}O_{10}(OH)_2 + 9.4H^+ + 0{\cdot}6H_2O \rightleftharpoons 2.85Al^{3+} + 0.85\ K^+ + 3.15H_4SiO$
Montmorrillonite (MgCa)	$Ca_{0.17}Mg_{0.34}Al_{1.66}Si_4O_{10}(OH)_2 + 6H^+ + 4H_2O \rightleftharpoons 1.66Al^{+3} + 0.17Ca^{+2} + 0.34\ Mg^{+2}$
Montmorrillonite (MgNa)	$Na_{0.34}Mg_{0.34}Al_{1.66}Si_4O_{10}(OH)_2 + 6H^+ + 4H_2O \rightleftharpoons 1.66Al^{+3} + 0.34\ Mg^{+2} + 0.34Na^+$
Nontronite (K)	$K_{0.34}Fe_{1.67}Al_{0.67}Si_{3.66}O_{10}(OH)_2 + 7.36H^+ + 2.64H_2O \rightleftharpoons 0.67Al^{+3} + 1.67Fe^{+3} + 0.34K^+$
Magnetite-III	$Fe^{III}{}_2\ Fe^{II}O_4 + 8H^+ \rightleftharpoons 2Fe^{+3} + Fe^{+2} + 4H_2O$
Haematite-III	$Fe^{III}{}_2O_3 + 6H^+ \rightleftharpoons 2Fe^{+3} + 3H_2O$
Goethite-III	$Fe^{III}O(OH) \rightleftharpoons + 3H^+ \rightleftharpoons Fe^{+3} + 2H_2O$
Epidote	$Ca_2Fe^{III}Al_2Si_3O_{12}(OH) + 13H^+ \rightleftharpoons 2Al^{+3} + 2Ca^{+2} + Fe^{+3} + 3H_4SiO_4$
Chamosite (Chlorite group)	$Fe^{II}{}_5Al(AlSi_3)O_{10}(OH)_8 + 16H^+ \rightleftharpoons 2Al^{3+} + 5Fe^{2+} + 3H_4SiO_4 + 6H_2O$
Kaolinite	$Al_2Si_2O_5(OH)_4 + 6H^+ \rightleftharpoons 2Al^{+3} + 2H4SiO4 + H_2O$
Calcite	$CaCO_3 + H^+ \rightleftharpoons HCO_3^- + Ca^{2+}$
Dolomite	$CaMg(CO_3)_2 + 2H^+ \rightleftharpoons 2HCO_3{-} + Ca^{2+} + Mg^{2+}$
Beidellite-K	$K_{0.34}Al_{2.34}Si_{3.66}O_{10}(OH)_2 + 7.36H^+ + 2.64H_2O \rightleftharpoons 2.34Al^{+3} + 0.34K^+ + 3.66H_4SiO_4$
Gases	
H_2	$H^+ + e^- \rightleftharpoons 0.5H_2$

precipitated was again chamosite, with a very low H_2 production of 0.003 mol (Fig. 7c and d) indicating that very reductive conditions also favour the precipitation of chamosite (R9).

4.4. Eh-T map of H_2 production

Fig. 8 shows an Eh–T map for H_2 production for the entire range of temperature (T = 130–200 °C) and redox potential (Eh = −100 to −300 mV). The temperature and redox potentials were evaluated at increments of 10 °C and 50 mV, respectively. Three main domains were observed according to the rate of H_2 production. The first is a low H_2 production domain at low temperatures and low Eh. In this domain, the oxidation of Fe^{2+} and the H_2 generation were limited, and the precipitation of chamosite (Fe^{2+} phase) was favoured. At low temperatures (130 °C), the rate of biotite dissolution was low, leading to a dissolution time of 246 years. The second domain is an intermediate H_2 production domain at high temperatures and intermediate to low Eh values. This is the most extended domain. The oxidation of Fe^{2+} was favoured but not complete, the magnetite (Fe^{2+}/Fe^{3+} phase) precipitation was dominant and the amount of H_2 produced tended to be intermediate. Here, the rate of H_2 generation was higher because the dissolution of biotite was faster with the increasing temperature. The third domain is characterised by high H_2 generation at high Eh values. In this case, a strong tendency existed for Fe oxidation; all Fe^{2+} released from the biotite was oxidised to Fe^{3+}, favouring high amounts of H_2 generation. The precipitation of pure Fe^{3+} secondary phases such as haematite was favoured.

4.5. H_2 generation with different PCO_2

The simulations with increasing PCO_2 from 0.1 MPa (alkalinity = 15 meq/kg) to 0.21 MPa (alkalinity = 30 meq/kg) showed no difference in the amount of H_2 generation. However, when the PCO_2 increased to 0.55 MPa (alkalinity = 60 meq/kg), an increase in H_2 from 51 mol to 75 mol was observed (Fig. 9). This is related to the precipitation of haematite ($Fe^{3+}{}_2O_3$) instead of magnetite ($Fe_2^{3+}Fe^{2+}O_4$). The increase in CO_2 in the solution decreased the pH and thus increased the Eh favouring more oxidative conditions. Because pH and Eh are closely connected parameters, when the pH decreases, the Eh increases, generating a less reductive environment and favouring the oxidation of

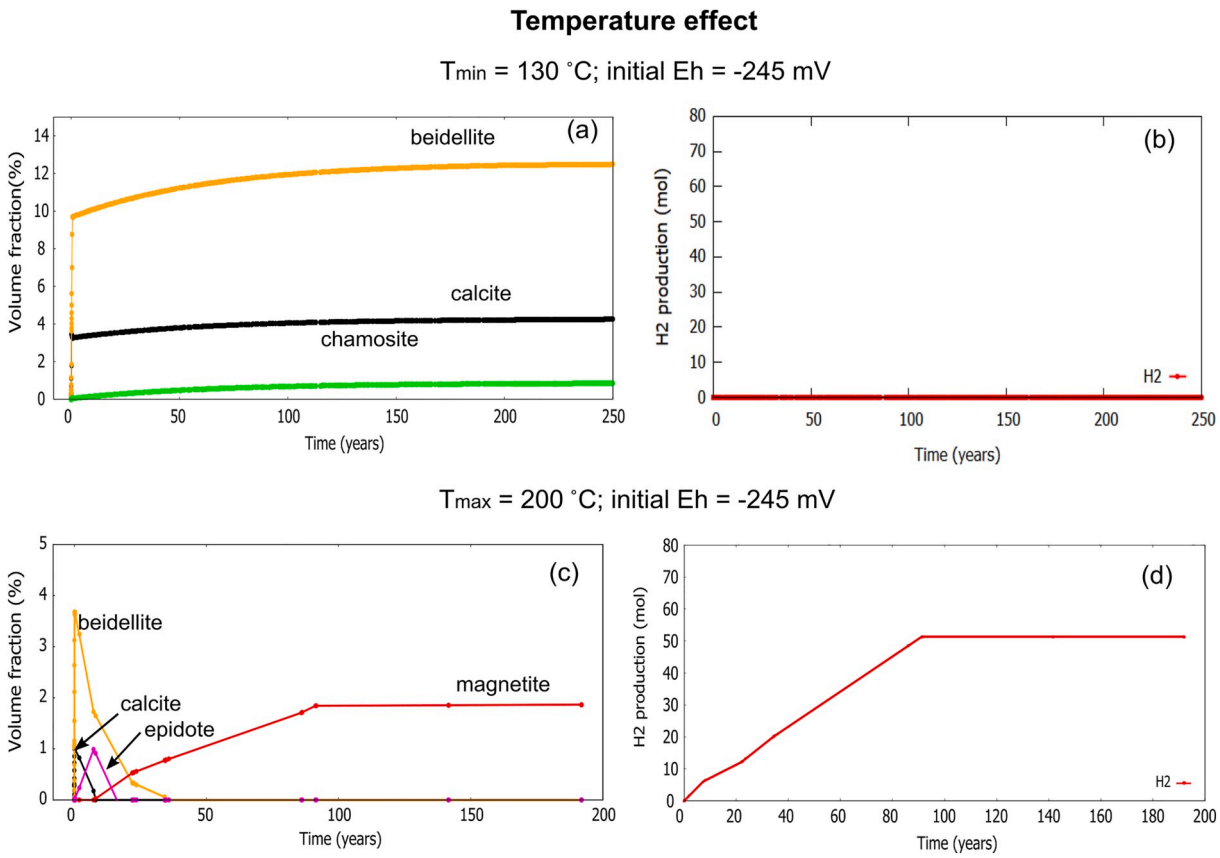

Fig. 6. Temperature effect on secondary minerals precipitation and H_2 production.

Fe^{2+} to Fe^{3+}, thus inducing a higher H_2 amount. When the PCO_2 increased to 1.13 MPa (alkalinity = 90 meq/kg), haematite continued to be the dominant phase, reaching equilibrium at pH = 4.7 and Eh = −241 mV.

5. Discussion

5.1. Hydrogen production

In this work, the results of simulations of the fluid–rock interaction in a 1 m^3 granitic cell that included the circulation of a natural heavy brine, revealed that abiotic H_2 can be generated during the hydrothermal alteration of the granite over a time scale of 100–200 years. Considering the influence of temperature on the kinetics of biotite dissolution, the time could vary from 91 years to 246 years according to the temperature range of the reservoir (130–200 °C). The alteration of biotite and the oxidation of Fe^{2+} to Fe^{3+} followed by the precipitation of Fe^{3+} phases in secondary minerals such as magnetite or haematite generated the needed redox reactions for H_2 generation. This H_2 generation process, which is generally referred to as 'reduction of water', is actually a reduction of protons (R6).

The evolution of primary and secondary minerals in the simulations were in agreement with the mineralogical descriptions of the natural hydrothermal alteration of the granitic rock. This corresponds to the dissolution of biotite, plagioclase, K-feldspar, and quartz associated with the precipitation of clay minerals (mainly illites, smectites, chlorites), carbonates (calcite and dolomite), and Fe oxides (Traineau et al., 1991; Genter and Traineau, 1992; Hooijkaas et al., 2006; Ledésert et al., 2010).

In our simulations, we applied different values of temperature and Eh for the geothermal brine as imposed variable conditions to test the behaviour of the mineral reactions, Fe^{2+}/Fe^{3+} redox reaction, and H_2 generation. Three domains were identified for the deep geothermal reservoir of Soultz-sous-Forêts. The first includes low Eh and low temperatures, in which Fe oxidation is limited; secondary Fe^{2+} phases such as chamosite precipitate, and H_2 generation is not possible. The second domain has higher Eh values, where Fe oxidation is favoured, and Fe^{3+} secondary phases such as haematite and goethite occur with the highest amount of H_2 produced, at 77 mol/m^3 of granite. In the third domain, at high temperatures and intermediate to low Eh values, which are dominant conditions of this site, the precipitation of Fe^{2+}/Fe^{3+} secondary phases such as magnetite is dominant with an intermediate H_2 production ratio of 51 mol/m^3 of granite.

Our simulations showed that the characteristic time scale for the alteration of biotite in the granite of Soultz-sous-Forêts, at 100–200 years, is considerably shorter than the age of the granite, at 330 Myr. Moreover, the present granite composition of Soultz-sous-Forêts is very rich in fresh or non-altered biotite (Hooijkaas et al., 2006). The biotite minerals show evidence of transformation into secondary minerals such as Fe oxides or chlorite only in the fractured zones of the granite and in propylitic alteration areas (Dezayes et al., 2005). This result indicates that if the granite is not exposed to disequilibrium conditions owing to fractures, temperature changes, and changes in the chemistry of fluids, the biotite remains in equilibrium. Accordingly, the potential of H_2 production is preserved until disequilibrium conditions are introduced.

5.2. Evolution of the brine

The minimal variation in the brine composition observed during the simulations is related to the equilibrium between the dissolution of primary minerals and the precipitation of secondary minerals. In all cases, the pH of the brine increased slightly from its initial value of 4.8 but remained in the range of the measured values of the in situ brine, at pH = 5 (Sanjuan et al., 2010). On the contrary, the initial Eh value of −245 mV tended to decrease to more negative values in all the

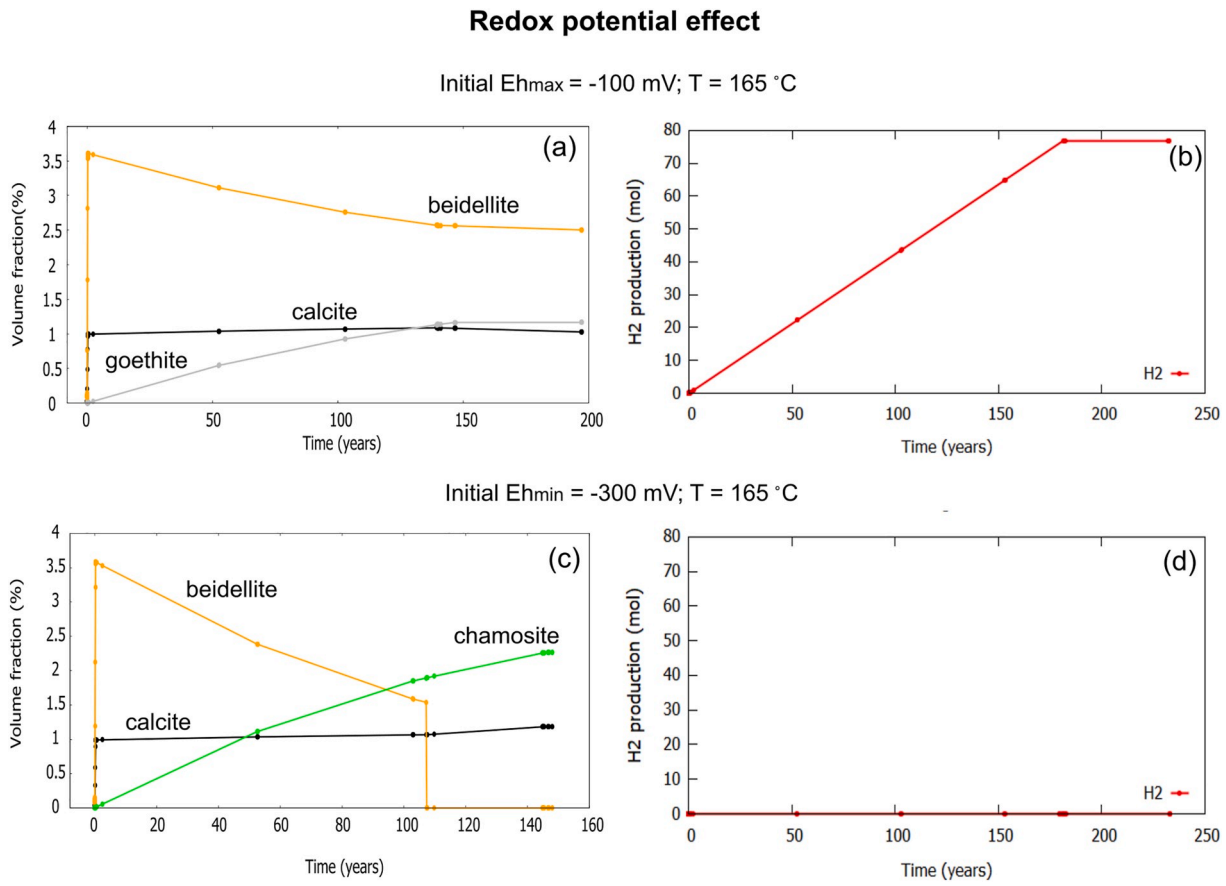

Fig. 7. Redox potential effect on secondary minerals precipitation and H_2 production.

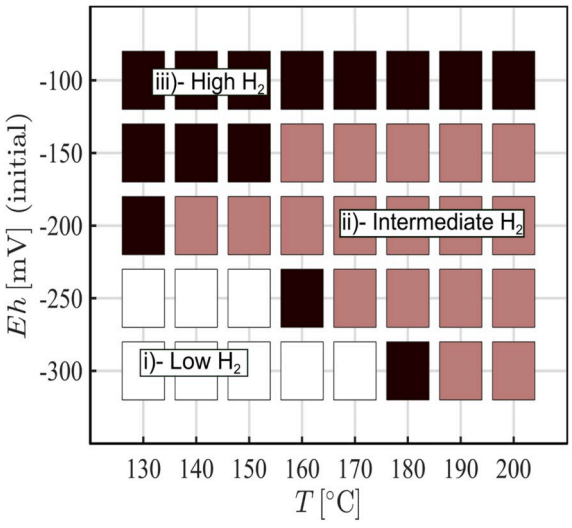

Fig. 8. Production of H_2 in the geothermal reservoir of Soultz-sous-Forêts combining different values of T and Eh.

simulations. The values of hydrothermal fluids measured during the last 20 years of exploration of the Soultz-sous-Forêts site do not show strong variation in the Eh value (Sanjuan et al., 2010, 2016). Therefore, H_2 generation does not appear to have a strong impact on the composition of the geothermal brine.

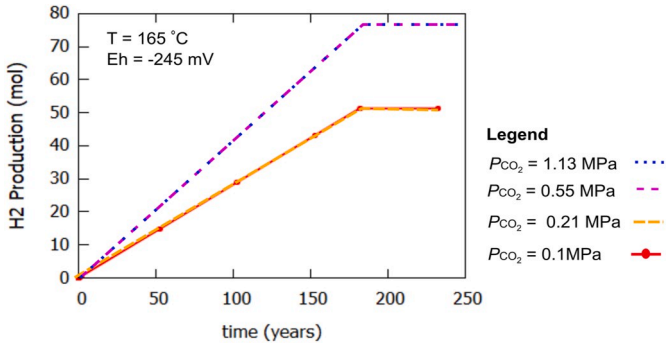

Fig. 9. Effect of P_{CO2} variation on H_2 production at T = 165 °C and Eh = -245 mV.

5.3. CO_2 effect

CO_2 is the dominant gas in the collected fluids from the granitic reservoir at Soultz-sous-Forêts. In this work, the calculated PCO_2 of the system was 0.1 MPa. With this pressure and the open system assumption, unlimited CO_2 is available to be dissolved in the solution. Therefore, CO_2 strongly regulates the pH of the brine and the precipitation–dissolution of calcite and clays. Although the production of H_2 contributes to proton consumption, the dissolution of CO_2 over time and the buffering effect by the re-dissolution of calcite and clays (beidellite-K) contribute to maintain a constant pH of about 5, which is in the range of the in situ brine (Sanjuan et al., 2010). By increasing the

PCO_2 in the system, the control on the pH is even stronger, and its effect on the increase of H_2 generation is observed. Indeed, this forces a decrease in pH and thus an increase in Eh to generate more oxidative conditions, which enhance Fe oxidation and H_2 generation. By increasing the PCO_2 (e.g. 0.55 MPa), a step was observed in the H_2 production with a significant increase in the rate over time (Fig. 9). The results of these simulations demonstrate that artificially increasing the PCO_2 of the system (i.e. by injection of CO_2) could improve the H_2 production.

5.4. Implications of the open system assumption

The open system assumption and constant PH_2 considered in this work implies that the amount of H_2 produced in the system can be calculated but with no control on the gas pressure changes or accumulation in the reservoir. As mentioned in section 3.1, the PH_2 value was calculated at the beginning of each simulation from the initial Eh and pH of the solution (Eq. (2)). In an Eh versus pH diagram for an open system (Fig. 10), PH_2 is represented as a line with a slope depending on temperature, which subsequently remained constant during the simulation even if the final pH and Eh changed from their initial values. In terms of minerals reactions, the assumption of an open system and constant PH_2 provides the conditions so that each time the H_2 gas is produced, it is exported from the system and thus maintains a constant PH_2. Considering reaction R8, if H_2 is exported, the reaction will tend to the right with the resulting biotite destabilization, magnetite precipitation, and H_2 production. The current hydrothermal forced circulation on the site allows us to consider that an open system and a constant PH_2 are valid assumptions for H_2 extraction.

In the case of a closed system assumption, any production of hydrogen will increase the local PH_2 partial pressure. As a feed-back effect, the reaction R8 would be pushed back to the left and biotite alteration would be inhibited preventing the production of H_2. This corresponds to what happened over the geological times in the geothermal reservoirs where the ferrous iron "survived". Therefore, a better understanding of the conditions that can lead to biotite destabilization to a large extent in the reservoir is needed. In simulations of H_2 production from ophiolites, the systems are open and the problem of partial gas pressure is sometimes resolved in modelling by using artificial modification of the solubility product of the involved gases. As such, a bi-phasic fluid is reduced to a monophasic fluid by considering H_2 not as a gas but as an aqueous specie dissolved in the solution ($H_{2(aq)}$; Bachaud et al., 2017). Mügler et al. (2016) used a thermodynamic model for the H_2 production coupled with a transport model for the bi-phasic fluid considering an open system with constant pressure. In our simulations we accounted for the amount of H_2 generation assuming an open system but with a mono-phasic fluid transport model. The H_2 modelling revealed the necessity of developing a two- or three-dimensional bi-phasic transport model whereby fluids and gases can be transported for undergoing thermodynamic and kinetic reactions.

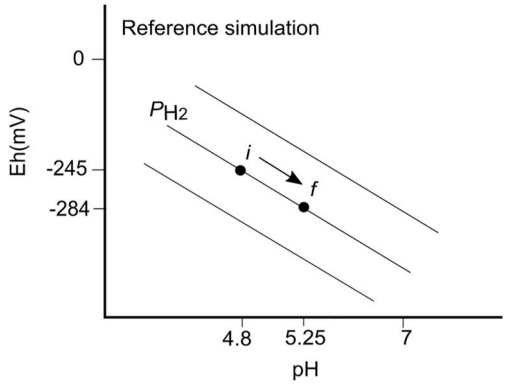

Fig. 10. pH-Eh diagram for an open system where PH_2 is represented as a line with a slope depending on temperature. PH_2 remains constant during the simulation from the beginning (*i*) to the end (*f*).

5.5. Comparison with H_2 production during serpentinisation of ultramafic rocks

Similarity was noted in the H_2 production processes during hydrothermal alteration of the granite and that of mafic rock during serpentinisation (Table 8). In both cases, the source of H_2 is related to the oxidation of Fe^{2+}-bearing minerals and the precipitation of Fe^{3+} in secondary minerals. In ultramafic rocks, the Fe^{2+} minerals are olivine $(MgFe^{2+})_2SiO_4$ and pyroxenes including clinopyroxene $(CaFeSi_2O_6)$ and orthopyroxene $(Mg,Fe^{2+})(Si_2O_6)$, whereas that in granite is biotite $(KFe^{2+}{}_3(AlSi_3)O_{10}(OH)_2)$. Amphibole can also be a source of Fe^{2+} in granites, although Mg-rich hornblende is the dominant amphibole type at Soultz-sous-Forêts. Because these mafic minerals contain different amounts of Fe^{2+} in their stoichiometry, the potential for H_2 generation is intrinsically different. When considering only the stoichiometry, biotite containing 3 mol Fe^{2+} per mol of biotite is richer in Fe^{2+} than olivine and pyroxenes containing 1 mol Fe^{2+} per mol of olivine or pyroxene in the richest Fe extreme of their crystallographic series. Therefore, the biotite has a greater potential for H_2 production. However, when considering the whole rock, peridotites have ≥60 wt% olivine, which is equivalent to ≥60 vol%, and pyroxenite rocks have ≤60 wt% olivine. In contrast, the maximum amount of biotite in the biotite-rich granite at Soultz-sous-Forêts is only 10 vol%, which is significantly lower.

The initial amount of Fe^{2+} in the primary rock is not the only important factor for H_2 production during serpentinisation in both deep mid-oceanic ridge and shallow ophiolite environments. Certainly, it is a complex process that depends on several parameters such as the physical–chemical composition of the circulating fluid, including temperature, pH, and silica activity; the primary mineral assemblage, including olivine/pyroxene ratio; and the water-to-rock ratio. These parameters determine the oxidation of the Fe^{2+} primary minerals, the partitioning of Fe in the secondary phases, the type of Fe (Fe^{2+}/Fe^{3+}) secondary mineral precipitation, and thus the H_2 production. Field and petrographic observations, laboratory experiments, and simulations of the serpentinisation process revealed that magnetite is a common secondary

Table 8
Comparative table for native H_2 production by serpentinisation of ultramafic rocks versus hydrothermal alteration of biotite-rich granite at Soultz-sous-Forêts.

Parameter	Serpentinisation of ultramafic rocks	Hydrothermal alteration of biotite-rich granite at Soultz-sous-Forêts
Primary Fe^{2+} mineral as source of H_2	olivine ($(MgFe^{2+})_2SiO_4$) pyroxene ($(CaFe^{2+})(Si_2O_6)$); ($(Mg,Fe^{2+})(Si_2O_6)$)	biotite ($KFe^{2+}{}_3(AlSi_3)O_{10}(OH)_2$) ± amphibole
Amount of primary Fe^{2+} minerals in the rock	peridotites ≥ ~60 vol% of olivine pyroxenite ≤ ~60 vol% of olivine	granite with ≈10 vol% of biotite
Secondary mineral associated to H_2 generation	magnetite ($Fe_2^{3+}Fe^{2+}O_4$) serpentinite ($(Mg,Fe^{3+})_{(3\text{-}Fe(III))}(SiFe^{3+})O_5(OH)_4$)	magnetite ($Fe_2^{3+}Fe^{2+}O_4$) goethite ($Fe^{3+}O(OH)$) epidote ($Ca_2Fe^{3+}Al_2Si_3O_{12}(OH)$)
Minerals limiting H_2 generation	brucite ($(Mg,Fe^{2+})(OH)_2$)	chamosite ($Fe^{2+}{}_5Al(AlSi_3)O_{10}(OH)_8$)
T for H_2 generation	20 to 350 °C	130 to 200 °C
pH	mainly alkaline, with some cases at ≈ 2.3	≈5
Eh	negative (mV)	−100 mV to −300 mV
Activity of Si	$10^{-2.5}$ to 10^{-5}	$10^{-2.6}$
fO_2	Extremely low	Extremely low

mineral associated with H_2 generation, whereas brucite ($(Mg,Fe^{2+})(OH)_2$) and serpentinite ($(Mg,Fe^{3+})_{(3\text{-}Fe(III))}(SiFe^{3+})O_5(OH)_4$) can limit or favour the production of H_2 accordingly (Charlou et al., 2002; McCollom and Bach, 2009; Marcaillou et al., 2011; Klein et al., 2013; McCollom et al., 2016; Bachaud et al., 2017; Miller et al., 2017; Vacquand et al., 2018). Similarly, at Soultz-sous-Forêts the most favourable conditions for H_2 are associated with magnetite precipitation, and the occurrence of Fe^{2+} phases such as chamosite at low temperatures inhibit the generation of H_2.

In serpentinisation, the low silica activity in the fluids of ultramafic rocks, on the order of $10^{-2.5}$ to 10^{-5}, results in the formation of alteration minerals, particularly serpentines and brucite. These minerals tend to largely exclude Fe^{2+} from their structure, leading to the formation of magnetite and thus H_2 (Frost and Beard, 2007; McCollom and Bach, 2009). In more silica-rich rocks such as basalts, a greater proportion of Fe^{2+} is sequestered in silicate alteration minerals such as chlorite and amphibole which allow Fe^{2+} into their structures. As a result, hydrothermal alteration of basalt generates significantly lower amounts of H_2 than that by serpentinisation of ultramafic rocks even though the Fe^{2+} content of basalt is typically much higher (McCollom and Bach, 2009). The silica activity in the aqueous fluid of the Soultz-sous-Forêts granite is about $10^{-2.6}$, which is higher than that in ultramafic rocks. In the granite, the precipitation of chlorite could be related to the higher silica activities, which limit H_2 generation. However, at temperatures $\geq$140 °C and Eh $\geq$ -250 mV, the silica activity does not appear to be a limiting condition for H_2 production because Fe oxides, specifically magnetite and haematite, are the dominant precipitation phases.

A wide range of temperature is possible for H_2 generation during serpentinisation. High temperatures of about 350 °C are found in mid-oceanic ridge vents (Charlou et al., 2002; McCollom et al., 2016), whereas those of about 20 °C can be found in ophiolite outcrops (Bachaud et al., 2017; Vacquand et al., 2018). In this sense, the range of temperatures at Soultz-sous-Forêts, 130–200 °C, reflects intermediate values compared with those occurring in serpentinisation.

Serpentinisation environments are dominated by alkaline solutions attributed to the dissolution of olivine and pyroxene (Seyfried et al., 2015, and references therein). However, H_2 is also produced in low-pH environments such as the Rainbow hydrothermal vent field, where exceptional pH values of ≈2.3 occur together with one of the highest H_2 concentrations detected in the Mid-Atlantic Ridge (MAR) system (Charlou et al., 2002). According to Allen and Seyfried (2003), the low pH at Rainbow is related to serpentinisation of pyroxene-rich lithologies rather than olivine. At Soultz-sous-Forêts the in situ brine has also a low pH of about 5, which has remained constant over time (Sanjuan et al., 2010). In all of our simulations, the pH remained at about 5, which produced H_2 at different temperature and Eh values accordingly. Moreover, when lower pH values were induced by increasing the P_{CO2}, higher H_2 generation was possible. In this case, a decrease in the pH value led to an increase in Eh. This resulted in less reductive conditions that favoured Fe^{2+} oxidation and the precipitation of Fe^{3+} secondary phases such as haematite and high amounts of H_2.

Low oxygen fugacity (fO_2) is also a distinctive condition during serpentinisation (Frost and Beard, 2007). In the Soultz-sous-Forêts case, the system had a very low O_2 content considering its depth of about 3500 m.

The values of H_2 produced by serpentinisation of ultramafic rocks in oceanic environments such as MAR vary at 0.02–16 mmol/kg (Charlou et al., 2002, and references therein). The calculated $H_{2(aq)}$ values in ophiolite systems such as those in Oman are about 0.008–0.01 mol/L (Bachaud et al., 2017). The amount of H_2 which could be produced by a granite reservoir is likely less than that produced by serpentinisation. However, the advantage of Soultz-sous-Forêts lies in its relative accessibility to the geothermal reservoir and the existence of a potential basement, where unaltered biotite occurs as a source of primary Fe^{2+} oxidation to produce H_2 as a by-product of the actual heating exchange system exploited to generate electricity.

5.6. Potential for abiotic H_2 generation at Soultz-sous-Forêts

In the intermediate H_2 production domain shown in Fig. 8, the amount of H_2 produced at high temperatures and intermediate to low Eh values is 51.2 mol per m^3 of granite. This quantity can be considered as the maximum potential of 1 m^3 of granite assuming complete dissolution of biotite and precipitation of magnetite. Under this assumption, an extrapolation can be made to the entire geothermal reservoir at Soultz-sous-Forêts. In this enhanced geothermal system, the volume of granite reached by the geothermal wells is approximately 1 km^3 (Fig. 11; Sausse et al., 2010). Therefore, the total potential of 1 km^3 of granite after the dissolution of all biotite and the precipitation of magnetite would be 51×10^9 mol or 102 kt H_2. This represents 0.2% of the total amount of H_2 produced and consumed worldwide annually, which is more than 55 Mt (Hydrogen Council, 2017).

However, this consideration is an upper bound because the conditions of temperature and Eh vary in the reservoir, and the natural circulating fluids and current exploitation methods will probably not achieve a complete disequilibrium of the whole volume of granite to extract all the calculated H_2 potential. Nevertheless, this is a valid and important data since it helps to dimension the potential of the site and to think about the production methods. For instance, artificial changes of PCO_2 by CO_2 injection could improve the amount of H_2 production as shown in simulations with increasing PCO_2 values (section 5.3.). The following question is then posed: how can an enhanced geothermal system serve as an active destabiliser of the biotite in a reservoir given that this mineral has survived over geological time in the quasi-closed system?

5.7. Other possible natural sources of H_2 at Soultz-sous-Forêts

5.7.1. Precipitation of sulphide (pyrite)

Pyrite, a sulphide mineral associated with hydrothermal alteration, occurs at Soultz-sous-Forêts at about 1 vol%. Despite the fact that pyrite is the most common sulphide on Earth, its formation involves complicated organic as well as inorganic mechanisms (Rickard and Luther, 2007). For inorganic reactions, it is widely accepted that pyrite is a secondary precipitated phase having an important influence on redox reactions. One common method for expressing this is described in reaction 10, in which pyrite is expected to form via nucleation and growth in solution. This reaction is favourable at about 300–350 °C (Rickard, 1997).

$$Fe^{2+} + 2S^{2-} \rightarrow FeS_2 + 2e^- \quad (R10)$$

In other cases, pyrite precipitation can occur from an existing S precursor reacting with sulphidic acid (R11). In this case, pyrite and H_2 can be produced in the presence of H_2S. Reaction 11, known as the Berzelius reaction, is favourable below 300 °C and can occur in aquatic sedimentary systems, buried sediments, and submarine fumaroles (Rickard, 1997; Rickard and Luther, 2007).

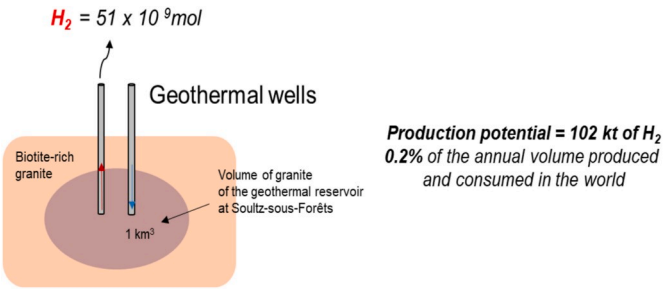

Fig. 11. Conceptual model for the maximum amount of H_2 production in the granitic geothermal reservoir of Soultz-sous-Forêts (1 km^3) in case of a complete dissolution of biotite and precipitation of magnetite.

$FeS(s) + H_2S = FeS_2(s) + H_2$ (R11)

Although the range of temperature of the hydrothermal system at Soultz suggests that reaction 11 could be favourable, the presence of precursors is not clear. Moreover, related equations and corresponding thermodynamic data are not introduced in KIRMAT to simulate this reaction. However, because pyrite has an important influence on redox reactions, future research should include this mineral in simulations to understand its effect on H_2 generation.

5.7.2. Radiolysis of water

The production of H_2 can also be linked to the radiolysis of water, in which the decay of K, Th, and U in rocks generates α, β, and γ radiation that dissociates water molecules in the rock pore spaces and fractures to form H_2 (Apps and van de Kamp, 1993; Lin et al., 2005; Lin et al., 2005). Lin et al. (2005) reported that radiolytic H_2 production rates in water range from 10^{-8} to 10^{-9} nM s^{-1} for granite, basalt, and quartzite lithologies. Sherwood Lollar et al. (2014) determined that the amount of H_2 generated via radiolysis and hydratation of the Precambrian continental lithosphere is similar to the estimated production from marine serpentinisation environments. Because the granite basement at Soultz-sous-Forêts is enriched in K, Th, and U (Pribnow et al., 1999; Pribnow and Schellschmidt, 2000; Baillieux et al., 2013) and radioactivity is known to contribute to the thermal anomaly, the production of H_2 related to radiolysis is a process worthy of future research.

6. Conclusion

The geochemical and reactive transport simulations conducted in this study indicate that generation of abiotic H_2 at Soultz-sous-Forêts is possible by hydrothermal alteration of the biotite as a source of Fe^{2+}, which is oxidised to Fe^{3+} leading to magnetite precipitation and a reduction of protons (H^+). By combining different temperature and Eh conditions relevant for the deep geothermal reservoir of Soultz-sous-Forêts, three main domains were identified: i) low H_2 generation domain, at low temperatures and very reductive Eh values where Fe^{2+} oxidation does not occur; ii) intermediate H_2 generation domain, at high temperatures and intermediate to low Eh with partial oxidation of Fe^{2+} to Fe^{2+}/Fe^{3+} secondary phases, mainly magnetite; iii) high H_2 domain, at high Eh values with strong tendency for Fe^{2+} oxidation and precipitation of pure Fe^{3+} phases. The second domain, was identified as the most extended and most likely for the system.

Our simulations also provide insight on the time scales involved in the H_2 generation processes occurring in the deep geothermal reservoir of Soultz-sous-Forêts. At conditions of 165 °C and −245 mV, the fresh standard porphyritic granite produced 51.3 mol/m^3 H_2 in 147 years after the complete dissolution of the total amount of biotite and the precipitation of magnetite. The process duration is remarkably fast compared with the age of the granite, at 330 Myr.

In the natural system biotite showed transformation to secondary minerals such as Fe oxides or chlorite only in the fractured zones of the granite and in the propylitic alteration areas, respectively. This indicates that unless the granite is exposed to disequilibrium conditions through fractures or changes in temperature or fluid chemistry, the biotite remains in equilibrium, maintaining strong potential for anthropogenic H_2 production. Simulations supports that an open system condition will favour H_2 production with a feedback effect on biotite disequilibrium and Fe^{2+} oxidation, while a closed system will limit the progression of the reaction and the H_2 production. Extrapolation to the entire volume of the geothermal reservoir of Soultz-sous-Forêts (estimated to be of the order of 1 km^3 of granite) indicates that the total H_2 potential after the dissolution of all biotite (with magnetite precipitation at 165 °C and −245 mV) is 51 × 10^9 mol or 102 kt H_2.

This number corresponds to a maximum if ideal conditions of new circulations of unbalanced geothermal fluids will be able to reach all the biotite of the reservoir. In reality, the conditions of temperature and Eh vary in the reservoir, and the natural circulating fluids and current exploitation methods will probably not achieve a complete disequilibrium of the whole volume of granite to extract all the assessed potential. However, this maximum potential represents 0.2% of the total amount of H_2 produced and consumed worldwide annually, which is more than 55 Mt. It constitutes an important number to be taken into account for future development of H_2 exploration in granitic basements and developments of production methods. Future research objectives should focus on understanding the exploitation conditions that can lead to the destabilization of a significant portion of the biotite in the reservoir in relation to the natural and engineered fracture networks. These conditions were obviously not experienced during the geological history of the reservoir since a large part of the biotite is still existing after several hundreds of million years (Hercynian granite). The destabilization process for H_2 production is expected to occur as a result of new geochemical disequilibrium caused by exploitation methods that will be able to activate the circulation in reopened or new fractures allowing the fluid to reach ferrous iron bearing minerals in open system condition. For instance, artificially increasing the PCO_2 by injection of CO_2 in the system can improve the amount of H_2. In particular, simulations showed that incremental increases in PCO_2 can indirectly induce Fe oxidation by changing the pH and Eh of the solution, resulting in more oxidant conditions that improved production of H_2. In addition, it is necessary in the future research to evaluate the extent to which the open system assumption and the imposed redox conditions influence the H_2 production at Soultz-sous-Forêts by a feedback effect on Fe^{2+} oxidation if an important part of the biotite mineral can be attained by the circulated fluid. This could be monitored and controlled in the currently exploited system.

Declararion of competing interest

The authors declare no conflicts of interest.

Acknowledgment

This work was supported by a grant from Total S.A. (No. DS5333SAV 17/EOT/223/01) as well as funding from LABEXANR-11-LABX-0050-G-EAU-THERMIE-PROFONDE, which is managed by the French National Research Agency as part of the 'Investments for the Future' program. We acknowledge to anonymous reviewers that contributed to improve the manuscript.

Appendix A. Supplementary data

Supplementary data to this article can be found online at https://doi.org/10.1016/j.apgeochem.2020.104631.

References

Allen, D.E., Seyfried, W.E.J., 2003. Compositional controls on vent fluids from ultramafic-hosted hydrothermal systems at mid-ocean ridges: an experimental study at 400 °C, 500 bars. Geochem. Cosmochim. Acta 67, 1531–1542. https://doi.org/10.1016/S0016-7037(02)01173-0.

Apps, J.A., van de Kamp, P.C., 1993. Energy gases of abiogenic origin in the earth's crust. In: Howell, D.G. (Ed.), The Future of Energy Gases, p. 890. USGS professional paper 1570.

Bachaud, P., Meiller, C., Brosse, E., Durand, I., Beaumont, V., 2017. Modeling of hydrogen genesis in ophiolite massif. Procedia Earth Planet. Sci. 17, 265–268. https://doi.org/10.1016/j.proeps.2016.12.051.

Baillieux, P., Schill, E., Edel, J.B., Mauri, G., 2013. Localization of temperature anomalies in the Upper Rhine Graben: insights from geophysics and neotectonic activity. Int. Geol. Rev. 55 (14), 1744–1762. https://doi.org/10.1080/00206814.2013.794914.

Blanc, P., 2017. Thermoddem: Update for the Version. Report BRGM/RP-66811-FR, p. 20.

Bresee, J.C., 1992. Geothermal energy in Europe: The Soultz Hot Dry Rock Project. CRC Press.

Charlou, J.-L., Donval, J.P., Fouquet, Y., Jean-Baptiste, P., Holm, N., 2002. Geochemistry of high H2 and CH4 vent fluids issuing from ultramafic rocks at the Rainbow hydrothermal field (36°14'N, MAR). Chem. Geol. 191, 345–359. https://doi.org/10.1016/S0009-2541(02)00134-1.

Dezayes, C., Chèvremont, P., Tourlière, B., Homeier, G., Genter, A., 2005. Geological Study of the GPK4 HFR Borehole and Correlation with the GPK3 Borehole (Soultz-Sous-Forêts, France). Final Report, BRGM Report. Orléans, France, RP-53697-FR.

Etiope, G., Samardžić, N., Grassa, F., Hrvatović, H., Miošić, N., Skopljak, F., 2017. Methane and hydrogen in hyperalkaline groundwaters of the serpentinized Dinaride ophiolite belt, Bosnia and Herzegovina. Appl. Geochem. 84, 286–296. https://doi.org/10.1016/j.apgeochem.2017.07.006.

Etiope, G., Sherwood Lollar, B., 2013. Abiotic Methane on Earth. Rev. Geophys., 51, 276–299. https://doi.org/10.1002/rog.20011.

Fritz, B., Jacquot, E., Jacquemont, B., Baldeyrou-Bailly, A., Rosener, M., Vidal, O., 2010. Geochemical modelling of fluid-rock interactions in the context of the Soultz-sous-Forêts geothermal system. CR Geosci 342, 653–667. https://doi.org/10.1016/j.crte.2010.02.005.

Frost, B.R., Beard, J.S., 2007. On silica activity and serpentinization. J. Petrol. 48, 1351–1368. https://doi.org/10.1093/petrology/egm021.

Ganor, J., Huston, T.J., Walter, L.M., 2005. Quartz precipitation kinetics at 180°C in NaCl solutions—implications for the usability of the principle of detailed balancing. Geochem. Cosmochim. Acta 69 (8), 2043–2056. https://doi.org/10.1016/j.gca.2004.09.026.

Genter, A., Traineau, H., 1992. Borehole EPS-1, Alsace, France: preliminary geological results from core analysis for Hot Dry Rock research. Sci. Drill. 3, 205–214.

Genter, A., Evans, K., Cuenot, N., Fritsch, D., Sanjuan, B., 2010. Contribution of the exploration of deep crystalline fractured reservoir of Soultz to the knowledge of enhanced geothermal systems (EGS). CR Geosci 342 (7–8), 502–516. https://doi.org/10.1016/j.crte.2010.01.006.

Gérard, F., Clément, A., Fritz, B., 1998. Numerical validation of an Eulerian hydrochemical code using a 1D multisolute mass transport system involving heterogeneous kinetically controlled reactions. J. Contam. Hydrol. 30, 201–216. https://doi.org/10.1016/S0169-7722(97)00047-.

Gérard, A., Genter, A., Kohl, T., Lutz, P., Rose, P., Rummel, F., 2006. The deep EGS (enhanced geothermal system) project at Soultz-sous-Forêts (Alsace, France). Geothermics 35 (5–6), 473–483. https://doi.org/10.1016/j.geothermics.2006.12.001.

Guélard, J., Beaumont, V., Rouchon, V., Guyot, F., Newell, K.D., Deville, E., 2017. Natural H2 in Kansas: deep or shallow origin? G-cubed 18, 1841–1865. https://doi.org/10.1002/2016GC006544.

Hooijkaas, G.R., Genter, A., Dezayes, C., 2006. Deep-seated geology of the granite intrusions at the Soultz EGS site based on data from 5 km-deep boreholes. Geothermics 35, 484–506. https://doi.org/10.1016/j.geothermics.2006.03.003.

Huenges, E., Ledru, P. (Eds.), 2011. Geothermal Energy Systems: Exploration, Development, and Utilization. John Wiley Sons, p. 486.

Hydrogen Council, 2017. Hydrogen Scaling up. A Sustainable Pathway for the Global Energy Transition, p. 78.

Kelley, D.S., Karson, J.A., Früh-Green, G.L., Yoerger, D.R., Shank, T.M., Butterfield, D.A., Hayes, J.M., Schrenk, M.O., Olson, E.J., Proskurowski, G., Jakuba, M., Bradley, A., Larson, B., Ludwig, K., Glickson, D., Buckman, K., Bradley, A.S., Brazelton, W.J., Roe, K., Elend, M.L., Delacour, A., Bernasconi, S.M., Lilley, M.D., Baross, J.A., Summons, R.E., Sylva, S.P., 2005. A serpentinite-hosted ecosystem: the lost city hydrothermal field. Science 307, 1428–1434. https://doi.org/10.1126/science.1102556.

Klein, F., Bach, W., Jöns, N., McCollom, T., Moskowitz, B., Berquó, T., 2009. Iron partitioning and hydrogen generation during serpentinization of abyssal peridotites from 15°N on the Mid-Atlantic Ridge. Geochem. Cosmochim. Acta 73, 6868–6893. https://doi.org/10.1016/j.gca.2009.08.021.

Klein, F., Bach, W., McCollom, T.M., 2013. Compositional controls on hydrogen generation during serpentinization of ultramafic rocks. Lithos 178, 55–69. https://doi.org/10.1016/j.lithos.2013.03.008.

Kohl, T., Evans, K.F., Hopkirk, R.J., Rybach, L., 1995. Coupled hydraulic, thermal and mechanical considerations for the simulation of hot dry rock reservoirs. Geothermics 345–359. https://doi.org/10.1016/0375-6505(95)00013-G.

Larin, N., Zgonnik, V., Rodina, S., Deville, E., Prinzhofer, A., Larin, V.N., 2015. Natural molecular hydrogen seepage associated with surficial, rounded depressions on the European craton in Russia. Nat. Resour. Res. 24, 369–383. https://doi.org/10.1007/s11053-014-9257-5.

Le Carlier, C., Royer, J. J, Flores Marquez, E. L, 1994. Convective heat transfer at the Soultzsous- Forêts geothermal site; implications for oil potential. First Break 12, 11, 553–560.

Ledésert, B., Hebert, R., Genter, A., Bartier, D., Clauer, N., Grall, C., 2010. Fractures, hydrothermal alterations and permeability in the Soultz Enhanced Geothermal System. C. R. Geosciences 342, 607–615. https://doi.org/10.1016/j.crte.2009.09.011.

Lin, L-H., Hall, J., Lippmann-Pipke, J., Ward, J.A., Sherwood Lollar, B., DeFlaun, M., Rothmel, R., Moser, D., Gihring, T.M, Mislowack, B., Onstott, T.C., 2005. Radiolytic H2 in continental crust: Nuclear power for deep subsurface microbial communities. Geochem. Geophys. Geosyst. 6, Q07003 https://doi.org/10.1029/2004GC000907.

Lin, L-H., Slater, G.F., Sherwood Lollar, B., Lacrampe-Couloume, G., Onstott, T.C., 2005. The yield and isotopic composition of radiolytic H2, a potential energy source for the deep subsurface biosphere. Geochimica et Cosmochimica Acta 69, 893–903. https://doi.org/10.1016/j.gca.2004.07.032.

Lu, S-M., 2018. A global review of enhanced geothermal system (EGS). Renewable and Sustainable Energy Reviews 81,, 2902–2921. https://doi.org/10.1016/j.rser.2017.06.097.

Magnenet, V., Fond, C., Genter, A., Schmittbuhl, J., 2014. Two-dimensional THM modelling of the large scale natural hydrothermal circulation at Soultz-sous-Forêts. Geoth. Energy 2. https://doi.org/10.1186/s40517-014-0017-x.

Marcaillou, C., Muñoz, M., Vidal, O., Parra, T., Harfouche, M., 2011. Mineralogical evidence for H2 degassing during serpentinization at 300°C/300bar. Earth Planet Sci. Lett. 303, 281–290. https://doi.org/10.1016/j.epsl.2011.01.006.

McCollom, T.M., Bach, W., 2009. Thermodynamic constraints on hydrogen generation during serpentinization of ultramafic rocks. Geochem. Cosmochim. Acta 73, 856–875. https://doi.org/10.1016/j.gca.2008.10.032.

McCollom, T.M., Seewald, J.S., 2013. Serpentinites, hydrogen, and life. Elements 9, 129–134. https://doi.org/10.2113/gselements.9.2.129.

McCollom, T.M., Klein, F., Robbins, M., Moskowitz, B., BerquóT, S., Jöns, N., Bach, W., Templeton, A., 2016. Temperature trends for reaction rates, hydrogen generation, and partitioning of iron during experimental serpentinization of olivine. Geochem. Cosmochim. Acta 181, 175–200. https://doi.org/10.1016/j.gca.2016.03.002.

McDermott, J.M., Seewald, J.S., German, C.R., Sylva, S.P., 2015. Pathways for abiotic organic synthesis at submarine hydrothermal fields. Proc. Natl. Acad. Sci. Unit. States Am. 112, 7668–7672. https://doi.org/10.1073/pnas.1506295112.

Miller, H.M., Mayhew, L.E., Ellison, E.T., Kelemen, P., Kubo, M., Templeton, A.S., 2017. Low temperature hydrogen production during experimental hydration of partially-serpentinized dunite. Geochem. Cosmochim. Acta 209, 161–183. https://doi.org/10.1016/j.gca.2017.04.022.

Mügler, C., Jean-Baptiste, P., Perez, F., Charlou, J.L., 2016. Modeling of hydrogen production by serpentinization in ultramafic-hosted hydrothermal systems: application to the Rainbow field. Geofluids 16, 476–489. https://doi.org/10.1111/gfl.12169.

Naumann, D., Zimmer, M., Erzinger, J., Wiersberg, T., 2000. Gas monitoring, fluid flux and fluid sampling at well GPK-2 (Soultz-sous-Forêts, France) – first results from the 5000m production test. Geotherm. Technol. - Geol. und energietechnische Ansatzpunkte 1, 71–84.

Olasolo, P., Juárez, M.C., Morales, M.P., Liarte, I.A., 2016. Enhanced geothermal systems (EGS): a review. Renew. Sustain. Energy Rev. 56, 133–144. https://doi.org/10.1016/j.rser.2015.11.031.

Palandri, J.L., Kharaka, Y.K., 2004. A Compilation of Rate Parameters of Water-Mineral Interaction Kinetics for Application to Geochemical Modeling (No. OPEN-FILE-2004-1068). Geological Survey Menlo Park CA.

Pauwels, H., Fouillac, C., Fouillac, A.M., 1993. Chemistry and isotopes of deep geothermal saline fluids in the Upper Rhine Graben: origin of compounds and water-rock interactions. Geochem. Cosmochim. Acta 57, 2737–2749. https://doi.org/10.1016/0016-7037(93)90387-C.

Pribnow, D., Fesche, W., Hägedorn, F., 1999. Heat Production and Temperature to 5 Km Depth at the HDR Site in Soultz-Sous-Forêts, p. 18. Hannover, NLfB - GGA report n°0 119 144.

Pribnow, D., Schellschmidt, R., 2000. Thermal tracking of upper crustal fluid flow in the Rhine Graben. Geophys. Res. Lett. 27 (13), 1957–1960. https://doi.org/10.1029/2000GL008494.

Rickard, D., 1997. Kinetics of pyrite formation by the H2S oxidation of iron (II) monosulfide in aqueous solutions between 25 and 125°C: the rate equation. Geochem. Cosmochim. Acta 61 (No. 1), 115–134. https://doi.org/10.1016/S0016-7037(96)00321-3.

Rickard, D., Luther, G.W., 2007. Chemistry of iron sulfides. Chem. Rev. 107, 514–562. https://doi.org/10.1021/cr0503658, 2007.

Rimstidt, J.D., Barnes, H.L., 1980. The kinetics of silica-water reactions. Geochem. Cosmochim. Acta 44, 1683–1699. https://doi.org/10.1016/0016-7037(80)90220-3.

Sanjuan, B., Millot, R., Innocent, C., Dezayes, C., Scheiber, J., Brach, M., 2016. Major geochemical characteristics of geothermal brines from the Upper Rhine Graben granitic basement with constraints on temperature and circulation. Chem. Geol. 428, 27–47. https://doi.org/10.1016/j.chemgeo.2016.02.021.

Rosener, M., Géraud, Y., 2007. Using physical properties to understand the porosity network geometry evolution in gradually altered granites in damage zones. Geol. Soc. London, Spec. Publ. 284, 175–184. https://doi.org/10.1144/SP284.12.

Sanjuan, B., Millot, R., Dezayes, C., Brach, M., 2010. Main characteristics of the deep geothermal brine (5 km) at Soultz-sous-Forêts (France) determined using geochemical and tracer test data. Compt. Rendus Geosci. 342, 546–559. https://doi.org/10.1016/j.crte.2009.10.009.

Sausse, J., Dezayes, C., Dorbath, L., Genter, A., Place, J., 2010. 3d model of fracture zones at Soultz-sous-Forêts based on geological data, image logs, induced microseismicity and vertical seismic profiles. Compt. Rendus Geosci. 342 (7–8), 531–545. https://doi.org/10.1016/j.crte.2010.01.011.

Sherwood Lollar, B., Onstott, T.C., Lacrampe-Couloume, G., Ballentine, C.J., 2014. The contribution of the Precambrian continental lithosphere to global H2 production. Nature 516, 379–382. https://doi.org/10.1038/nature14017.

Schindler, M., Baumgärtner, J., Gandy, T., Hauffe, P., Hettkamp, T., Menzel, H., Penzkofer, P., Teza, D., Tischner, T., Wahl, G., 2010. Successful hydraulic stimulation techniques for electric power production in the Upper Rhine Graben, Central Europe. In Proc. World Geother. Cong., Bali, Indonesia, 7pp.

Seyfried, W.E., Pester, N.J., Tutolo, B.M., Ding, K., 2015. The Lost City hydrothermal system: constraints imposed by vent fluid chemistry and reaction path models on subseafloor heat and mass transfer processes. Geochem. Cosmochim. Acta 163, 59–79. https://doi.org/10.1016/j.gca.2015.04.040.

Smith, N.J.P., Shepherd, T.J., Styles, M.T., Williams, G.M., 2005. Hydrogen Exploration: a Review of Global Hydrogen Accumulations and Implications for Prospective Areas in NW Europe, Petroleum Geology: North-West Europe and Global Perspectives—Proceedings of the 6th Petroleum Geology Conference. Geological Society, London, pp. 349–358.

Surma, F., Géraud, Y., 2003. Porosity and thermal conductivity of the Soultz-sous-Forêts granite. Pure Appl. Geophys. 160, 1125–1136. https://doi.org/10.1007/PL00012564.

Traineau, H., Genter, A., Cautru, J.P., Fabriol, H., Chèvremont, P., 1991. Petrography of the granite massif from drill cuttings analysis and well log interpretation in the geothermal HDR borehole GPK1 (Soultz-sous- Forêts, Alsace, France). Geoth. Sci. Technol. 3, 1–29.

Vallier, B., Magnenet, V., Schmittbuhl, J., Fond, C., 2019. Large scale hydro-thermal circulation in the deep geothermal reservoir of Soultz-sous-Forêts (France). Geothermics 78, 154–169. https://doi.org/10.1016/j.geothermics.2018.12.002.

Vacquand, C., Deville, E., Beaumont, V., Guyot, F., Sissmann, O., Pillot, D., Arcilla, C., Prinzhofer, A., 2018. Reduced gas seepages in ophiolitic complexes: evidences for multiple origins of the H2-CH4-N2 gas mixtures. Geochem. Cosmochim. Acta 223, 437–461. https://doi.org/10.1016/j.gca.2017.12.018.

Villemin, T., Bergerat, F., 1987. L'évolution structurale du fossé rhénan au cours du Cénozoique : un bilan de la déformation et des effets thermiques de l'extension. Bulletin de la société géologique de France. série 8, 3, 245–255.

Zgonnik, V., Beaumont, V., Deville, E., Larin, N., Pillot, D., Farrell, K.M., 2015. Evidence for natural molecular hydrogen seepage associated with Carolina bays (surficial, ovoid depressions on the Atlantic Coastal Plain, Province of the USA). Prog. Earth Planet. Sci. 2, 31 https://doi.org/10.1186/s40645-015-0062-5.